Copyright © 1998, by the International Council of the Aeronautical Sciences (ICAS)
and the American Institute of Aeronautics and Astronautics, Inc.

A98-31498

ICAS-98-2,3,1

AERODYNAMIC DESIGN OPTIMISATION APPLIED TO CIVIL TRANSPORTS WITH UNDERWING MOUNTED ENGINES

K.C.Hackett, DERA, Bedford, UK
P.H.Rees, BAe Airbus Ltd, Woodford, UK
J.K.Chu, BAe Airbus Ltd, Woodford, UK

Abstract

The problem of achieving an aerodynamically successful nacelle installation can be particularly difficult in the case of Long Duct Mixed Flow (LDMF) nacelles. Very large interference drag penalties can arise if an integrated design approach is not applied. LDMF nacelles have the benefit of reducing noise and improving specific fuel consumption due to the mixing process of the fan and core exhaust gases. Consequently, using an example of this type of nacelle, this paper describes an investigation that was undertaken with the following aims:

- By wind tunnel testing, to investigate the effect on installation of aerodynamic parameters such as Reynolds number, Mach number, and geometric parameters such as degree of wing/nacelle coupling, and pylon/nacelle alignment.
- To assess CFD analysis methods for their ability to predict the aerodynamic effects of varying the key geometric parameters associated with closely-coupled engine installations.
- By using conventional design techniques, and engineering judgement, to design a wing which is tolerant to closely-coupled engine installations.
- To develop and demonstrate an automated design-optimisation-methodology targeted at minimising interference effects.

1.0 Introduction

Technologies aimed at providing aircraft with the lowest possible Direct Operating Costs (DOC) continue to be the key to the design and operation of successful civil aircraft. The reduction of drag becomes more important with the increase in the proportion of fuel prices to DOC. Even when fuel prices are low the threat of increasing fuel prices presents an uncertainty in the future operation, planning and profitability of airline companies. Hence, there is a continuing desire to achieve the lowest possible drag to reduce that dependency.

The aerodynamic performance of civil aircraft suffers from the averse effects of interference drag between distinctive aircraft components. For example, the wing, nacelle, fuselage etc., if each had been separately designed and optimised without sufficient account being taken of their mutual interference. An example of this is the relatively large Long Duct Mixed Flow (LDMF) nacelle in close proximity to the wing which results in strong aerodynamic interaction between nacelle, pylon and the wing. These interference effects may manifest themselves in a number of ways which are:

- Non-optimal loading distributions giving rise to additional lift-induced (vortex) drag.
- The change in the development of supercritical flows, leading to the possible appearance of, or modification to strong shock waves resulting in an increase in wave drag and possibly viscous drag due to local flow separations.

Techniques to reduce the interference drag have been proposed. However, these have been confined generally to local treatment in the gully region inboard of the nacelle, pylon and the wing lower surface. Kutney proposed a cambered pylon with a fairing designed to prevent the airflow from attaining supersonic velocities during subsonic flight conditions[1,2]. Ogilvie et al designed a fairing which was positioned so that the cross sectional area of the gully is reduced and the revised wing lower surface region within the channel presented little or no chordwise curvature[3]. The addition of pylon extension fairing to reduce the lift loss due to the presence of the pylon has been shown to be a useful technique to reduce interference drag[4].

In recent years transonic Computational Fluid Dynamics (CFD) analysis methods have become available. These methods together with the appropriate supercomputing power, provide the ability to model flow around full aircraft configurations. Recently CFD methods have been used to study the interference effects of Ultra-High Bypass (UHB) engines mounted on wings[5,6]. Lynch identified the current role of CFD in addressing airframe/engine integration issues for subsonic transport at ICAS 94[7].

For future civil aircraft, particularly regional jets, there will be a desire to place the nacelle close to the wing due to restrictions placed on main undercarriage leg length and access to passenger entry and underfloor baggage doors. These requirements can also lead to the need to

Copyright © 1998 by ICAS and AIAA. All rights reserved

Copyright © 1998, by the International Council of the Aeronautical Sciences (ICAS)
and the American Institute of Aeronautics and Astronautics, Inc.

move the engine as far aft as possible. To have a better understanding of the elements in the interference process, a major programme of research involving collaboration between BAe and DERA, was started in 1995. The objective of the study is to investigate the aerodynamic design optimisation process when applied to civil transports with underwing mounted engines. The investigation involves a combination of experimental test, CFD validation and design optimisation. The use of CFD methods to model full aircraft configurations that are validated against experimental data will provide a means to develop the capability to optimise the design of close-coupled underwing engine installations. This capability is of particular interest where the introduction of CFD techniques allied with the design optimisation will reduce design cost and timescales.

This paper gives details of the progress of the study. Section 2 describes the pylon-nacelle designs to be investigated. Section 3 covers the comparison of various CFD codes used in the UK. Section 4 covers the experimental investigation and section 5 describes the comparisons with CFD predictions. The integrated wing design exercise is described in section 6. Finally, conclusions and future work is covered in sections 7 and 8.

2.0 Pylon/nacelle design

The vehicle chosen for this research programme is the wing and fuselage of an existing wind tunnel half-model, representative of a low-wing, twin-engine civil jet transport (design Mach number = 0.78). This model had the benefit of having a pressure-plotted wing and was capable of being tested in a pressurised wind tunnel. The nacelle and associated support pylons were newly designed components for this programme.

The nacelle, having a desired favourable pressure distribution along its length for the isolated nacelle case, is an axisymmetric through-flow representation of a conventional LDMF turbofan design. The external shape is composed of (i) a forward profile from the highlight back to maximum diameter followed by (ii) a circular arc which blends into (iii) a conical boat-tail of semi-angle 11°. The internal duct comprises a convergent conical region of 5° semi-angle, which forms a tangent to the inner front lip followed by a cylindrical bore which extends back to the nozzle exit. The design ensures the internal flow remains attached.

The exit area/highlight area ratio achieved was 0.61 which ensured representative inlet flow stream.

Generally, for the datum configuration, the nacelle centre line was maintained parallel to the fuselage centre line in side view and aligned line-of-flight in plan view, (see Fig 10).

As shown in Fig. 1, the engine pylon design is integrally blended with a notional flap track fairing which extends beyond the wing trailing edge. In plan view the pylon to wing intersection is essentially parallel-sided along the wing chord, with the rear taper closure being applied aft of the wing trailing edge. The pylon crown (top) ahead of the wing approximates a flattened ellipse.

Initially, a datum nacelle position was selected similar to an A320/V2500 installation in terms of wing leading edge to nacelle exit overlap and wing to nacelle gap. Alternative nacelle locations selected for study included a forward shift, an aft shift and two successively raised positions. The most highly raised position 0, (Fig 1), was tested with both an under wing leading edge type pylon and also an over wing leading edge type pylon. It was considered that the extreme raised position may have led to a pylon structural box depth requirement which necessitated a pylon/wing upper surface intersection.

The pylon was mounted just inboard of the wing planform crank and was canted to be approximately normal to the dihedral of the wing plane, thereby relieving junction corner flows.

Separate pylons of similar generic design were designed and manufactured for each of the 5 nacelle positions (plus one additional over the wing leading edge pylon). A comparison of nacelle positions with some in-service aircraft fitted with LDMF nacelles is shown in Fig. 2.

For the wind tunnel model the nacelle was pressure-tapped externally at 3 radial stations disposed at 25° (top outboard), 180° (bottom) and 335° (top inboard) relative to the nacelle top centre line. The nacelle duct was also pressure plotted to determine intake mass flow ratio and internal drag.

3.0 Comparison of CFD Methods

As a first stage in the validation process of CFD methods, it is necessary to gain confidence in the inviscid solutions for complex configurations. To achieve this it is necessary to ensure that surface and field grids provide adequate resolution and that the flow solution are well converged.

Consequently, as part of the process comparisons have been made of results from three different CFD codes commonly used in the UK: RANSMB[8,9,10], FLITE3D[11,12] and SAUNA[13]. RANSMB (Reynolds-Averaged Navier-Stokes Multi-Block) is a British Aerospace CFD code, which allows a range of several different turbulence models to be employed, or application can be run in inviscid Euler mode. This method solves the flow equations at cell centres. FLITE3D is an unstructured grid method (currently inviscid) developed by Swansea University in

Copyright © 1998, by the International Council of the Aeronautical Sciences (ICAS)
and the American Institute of Aeronautics and Astronautics, Inc.

conjunction with British Aerospace. SAUNA was developed under contract to DERA by the Aircraft Research Association (ARA) and is a hybrid method with the capability to embed unstructured grids around surfaces with high geometric or flow complexity. This allows the benefits of reliable and affordable flow-solvers for structured grids to be retained, whilst utilising the added benefits of unstructured grids. Like RANSMB, SAUNA can be run in Euler, Euler viscous-coupled or Navier-Stokes mode. Unlike RANSMB, SAUNA is a cell-vertex scheme.

3.1 Wing plus Fuselage Configuration

The model fuselage consists of an axisymmetric nose, with cylindrical mid-body and an upswept rear portion. The wing/fuselage combination incorporates a wing leading edge root fillet (onglet) and a wing root trailing edge fairing which was defined as part of the fuselage.

It was originally intended that geometries for the three methods would be identical, but because of differences in the ability of the codes to generate suitable grids, it became necessary to accept small geometry modifications.

Initial calculations were made for the wing/body configuration illustrated in Fig. 3 which shows the surface grid employed with SAUNA.

Fig. 4 shows a comparison of wing pressure distributions on the inner wing in the region of the nacelle pylon position for M = 0.78, $\alpha = 2^{\circ}$. For reference, the planform trailing edge kink is located at exposed spanwise position $\eta_{net} = 0.311$ and the nacelle/pylon (when fitted) is at $\eta_{net} = 0.260$.

The shock development is well resolved by all methods with FLITE3D, the unstructured grid method giving the most upstream location and SAUNA the greatest pressure rise through the shock. On the lower surface all the methods agree well. The overall lift coefficients were found to agree well (Table 1), though there were large differences in drag obtained by integration of surface pressures. Since inviscid flow is prescribed, calculated drags comprise vortex drag and wave drag only. The reasons for the drag differences are explained in the next section. Also shown in the table is the result of SAUNA with the same grid as used for the RANSMB run thereby allowing effects of flow code differences alone to be assessed.

3.2 Wing/Body/Pylon/Nacelle Configuration

For the complete configuration, which is illustrated by the SAUNA surface grid in Fig. 5, the three CFD methods were applied to each of three cases where the nacelle was shifted forwards (P1/2) and aft (P1/4) relative to the datum position (P1/3), (see Fig 1). SAUNA used a hybrid grid with unstructured elements in the region of the pylon as illustrated in Fig. 6.

It was considered that a through-flow nacelle representation was adequate for the case of a LDMF type nacelle where jet interference effects are believed to be less important.

At conditions where compressibility effects are insignificant, wing pressure distributions close to the pylon calculated at M = 0.5, $\alpha = 2^{\circ}$ showed generally very good agreement. The effect of the nacelle on the wing lower surface pressures is seen to be relatively benign. (Fig. 7).

At M = 0.78, $\alpha = 1^{\circ}$, the comparison of wing pressures for the datum nacelle position either side of the pylon is shown in Fig 8. (The nacelle and pylon is located spanwise at $\eta_{net} = 0.260$). At this condition, the lower surface shock inboard of the pylon (sometimes referred to as the gully shock) is well resolved by all three methods. The upper surface shows some small difference of forward shock position between SAUNA and the other two methods.

The effect of the nacelle shift to positions P1/2 and P1/4 on wing pressures immediately either side of the pylon can be seen in Figs. 9a, 9b. It is evident from all three methods that the shock on the inboard lower surface moves aft and strengthens as the nacelle moves aft. However, the rate that the shock moves chordwise is about half the rate at which the nacelle moves.

Comparison of overall lift and drag forces at M=0.78, $\alpha = 1^{\circ}$ is shown in Table 2. The differences between the results of the methods may be ascribed to the different geometric treatments to the wing tip and wing root fairing (as described previously). FLITE3D is known to have a deficiency in drag calculation and this is currently under further development.

In light of the above, it is reasonable to judge the level of agreement of the methods by considering increments in force coefficients due to shifting the nacelle away from the datum position (Table 3). Presented are ΔC_D, ΔC_L and the change in drag, ΔC_{DI}, with the lift dependent term ($C_L^2/\pi A$) removed, where A is wing aspect ratio. The methods are in broad agreement in predicting the delta drag in changing to P1/2, but not so for P1/4 where lower surface shock strength becomes predominant. Although providing slightly disappointing results in terms of the effect of nacelle shift on forces, it does serve to highlight the difficulties in obtaining drag values for such complex flows, and perhaps indicates the need for a better resolution of the flow in critical regions. It also highlights the problems associated with using integrated pressures to calculate drag due to inherent numerical inaccuracy

Copyright © 1998, by the International Council of the Aeronautical Sciences (ICAS)
and the American Institute of Aeronautics and Astronautics, Inc.

depending on mesh densities.

4.0 Test in DERA 8 foot Transonic Tunnel

The tests were conducted in the 8ft x 8ft High-Speed Wind Tunnel facility at DERA Bedford, where overall force, moment and surface pressure measurements were recorded. The test did not model the jet effect because it is believed to be unimportant, and would have resulted in an expensive and lengthy wind tunnel programme.

The model was mounted onto a half model balance in the sidewall of the tunnel. The centre-line of the fuselage was displaced 25mm from the sidewall and a boundary-layer diverter added to minimise wall boundary-layer effects. Details of the model installation are shown in Fig 10 and the model reference dimensions are given in Table 4.

The test provided data of model forces and pressures for a variation of nacelle position, nacelle pitch and pylon yaw. The tests were performed at Mach numbers between 0.50 and 0.82, with Reynolds number per foot ranging from 4.1×10^6 to 8.2×10^6. Boundary-layer transition was fixed by ballotini applied to the upper surface at 15% chord and the lower surface at 5% chord.

Figs 11, 12 summarise the drag of the nacelle/pylon installation for a range of positions relative to the datum nacelle position (P1/3). Nacelle-pylon installation drag ($\Delta C_{D\ Installn}$) is defined as the drag increment at constant C_L resulting from the addition of the engine installation to the clean wing. Generally low installation drags were measured with the forward nacelle position (position P1/2) and it is found that adverse nacelle interference effects increased as the nacelle was moved aft (position P1/4).

The distribution of pressure tappings (along the chord of the wing lower surface) in the nacelle/pylon region are such that the fine details of the flow features cannot be captured. However, it can be deduced that large wing/nacelle overlaps has increased the wing lower surface shock due to the presence of a significant local separation bubble aft of the shock, Fig 13.

The close-coupled position P1/0, with under-wing leading edge pylon intersection produced a low installation drag relative to the datum position. Inspection of the surface pressures shows a reduction of lower surface shock strength with no evidence of a local separation bubble. It is surmised that the low drag must be due to the subtle effects of the pylon boat-tail shaping and the location of the blend details relative to the wing and nacelle.

Pylon/nacelle interference drag ($\Delta C_{D\ Interf}$) is that part of the engine installation drag which cannot be accounted for by simple drag estimation methods. This component is calculated by removing the estimated drag due to respective pylon/nacelle components from the measured increment in drag due to the addition of the engine installation to the clean wing. The pylon/nacelle interference drag ranges typically from $\Delta C_{D\ Interf} = 0.0007$ for position P1/2 to 0.0015 for position P1/4 (at the wing design condition).

Allowing the pylon top to pass over the wing leading edge and intersect the wing upper surface (P2/0), produced a significant interference drag penalty of $\Delta C_{DInterf} = 0.0010$ at the wing design condition of Mach 0.78, $C_L = 0.55$. This pylon type was found to produce a very high wing leading edge suction peak just inboard of the pylon. Therefore the shape of the overwing pylon needs to be revised to eliminate this feature.

Toeing the pylon/nacelle assembly inboard or outboard by $\pm 1.5^0$ produced a drag penalty relative to zero toe. Increasing the nacelle pitch from 0^o to 2.5^o generally caused a drag increase of about $\Delta C_{D\ Interf} = 0.00025$.

The effect of Reynolds number on interference drag was investigated with the datum nacelle position. Both the clean wing and datum were tested at Reynolds numbers of 4.1×10^6, 6.0×10^6, and 8.2×10^6 per ft and Fig 14 shows that the interference drag increases with Reynolds number.

The nacelle pressure distribution on the top inboard side, Fig 15, exhibits a suction peak towards the rear that reflects the mutual interference with the wing lower surface immediately inboard of the pylon. Nacelle trailing edge pressures in this region suggest the presence of shock-induced trailing edge separation at M=0.80, which becomes more severe with nacelle aft movement.

5 Comparison of CFD with experiment

During the course of the research programme the RANSMB Navier-Stokes code was progressively developed by BAe. Together with the availability of a CRAY T3D (with 256 processors), it became practicable to favour the use of the Navier-Stokes code over the Euler viscous coupled version of the code. The Navier-Stokes field grids differed from those used for the equivalent Euler inviscid investigation by having an increased density within the first grid block next to the wall. Calculations with k-g turbulence modelling[14] have been performed for wing/body (w/b) and for wing/body/pylon/nacelle (w/b/p/n) in each of the 5 nacelle positions (positions 0,1,2,3,4, Fig 1). The wing root leading edge fillet (onglet) was modelled as part of the wing and the wing trailing edge fairing was modelled as part of the fuselage as for the inviscid CFD cases considered earlier. The conditions selected corresponded with certain of the wind tunnel tests which formed part of the programme:

Copyright © 1998, by the International Council of the Aeronautical Sciences (ICAS)
and the American Institute of Aeronautics and Astronautics, Inc.

- M = 0.78
- $\alpha = 0^\circ, 1^\circ, 2^\circ$
- Re = 4.68×10^6 based on aerodynamic mean chord (amc)
- Transition = 15% /5% on wing upper/lower surface

A view of the surface grid can be seen in Fig. 16.

5.1 Viscosity Effects

It is well known that the effects of viscosity on inviscid CFD calculations are generally to reduce shock strengths and to cause wing upper surface shocks to move forwards. These effects can be clearly seen in a comparison of RANSMB Inviscid against the Navier-Stokes version at the station inboard of the pylon (Fig. 17). It is evident that the gully shock has also been weakened by the effects of viscosity.

5.2 Forces

Drag values obtained from RANSMB comprise integrated surface pressure drag plus skin friction drag. Direct comparison of drag from CFD with the measured wind tunnel results of a half-model is not meaningful, and so no attempt has been made to correlate them. Of more interest to the design engineer is the degree of agreement between CFD and wind tunnel results for the effect of nacelle movement on drag. Fig. 18 shows that RANSMB accurately predicts that the two most closely coupled nacelle positions (P1/0, P1/1) had a very small effect, relative to the nacelle datum position, on overall drag in the range of interest between C_L =0.3 and 0.5. Position 4 (aft position) was predicted to show a drag penalty of between $\Delta C_{D\ Installn}$ = 0.00025 and 0.00055, whereas wind tunnel results showed a penalty of $\Delta C_{D Installn}$ = 0.0007 to 0.0008. The most significant discrepancy occurred for position 2 (forward position) where RANSMB predicts a benefit of 3-6 drag counts. In practice it was found to be much smaller or even a slight penalty for lift coefficients greater than 0.40.

An attempt to understand the contribution of wave drag to nacelle installation drag led to Figs. 19a, 19b. These show the RANSMB N-S results for wing upper and lower surface wave drag calculated by a field method for w/b and w/b/p/n for each of the nacelle positions. Table 4 presents the same data numerically. This shows that for a fixed incidence, starting with position P3, raising the nacelle progressively through P1 and then P0 has no effect on upper surface wave drag and that lower surface "gully" drag actually tends to decrease. This is in agreement with the trend of total drag from RANSMB seen earlier. Progressive movement of the nacelle aft from position P1/2 through P1/3 to P1/4 shows both upper and lower surface "gully" drag to increase and for C_L to decrease. It appears that an increase in gully wave drag tends to be mirrored by an increase in wing upper surface wave drag. Conceptually, this could perhaps be understood as a result of the blocking of flow through the gully because of the gully shock, leading to more air being forced over the wing upper surface.

At $\alpha = 2^\circ$ where C_L = 0.52 to 0.53 depending on nacelle position (Fig. 19b), gully drag is obviously much reduced and wing upper surface wave drag is dominant.

Analysis of component forces in the CFD runs for each nacelle position reveals that for M=0.78, α=0,1,2, the nacelle always experiences a negative lift. This, of course, is additional to the negative lift increment induced on the wing due to the nacelle installation. Furthermore, the pylon always experiences a side force directed inwards, presumably because of the wing inboard lower surface suction peak. All these effects run counter to what is preferred for minimum installation drag.

5.3 Wing Spanwise Load Grading

The loss of a number of pressure tappings on the model wing prevented the derivation of spanwise lift variation due to the nacelle installation. However, the CFD results are presented for each of the different nacelle positions in Figs 20a to 20c. The effect of adding the nacelle at position P1/3 at constant $\alpha = 1^\circ$ (Fig. 20a) shows that the lift loss extends across the whole span. The greatest lift loss occurs just inboard of the pylon. This is a reflection of the increased lower surface suction associated with the gully shock. The effect of progressively raising the nacelle position from P1/3 though P1/1 to P1/0 is to reduce the spanwise lift loss (Fig. 20b). Moving the nacelle forward from P1/3 to P1/2 also reduces the lift loss. This is due to a weakening of the gully shock just inboard of the pylon and hence a reduction of the wing lower surface lift loss. Conversely, moving the nacelle aft to P1/4 increases the lift loss, especially at the pylon station, but again its effect propagates across the whole span. (Fig. 20c).

5.4 Wing Chordwise Pressure Distributions

A comparison of inboard wing pressures measured on the wind tunnel model with those predicted for the w/b configuration at M = 0.78, $\alpha = 2.0^\circ$ (C_L = 0.53 approx.) is shown in Fig. 21. The wing upper surface shock position and strength is well predicted. The poorer agreement at the station immediately adjacent to the root is probably due to discrepancies between model and CFD geometries of the wing root onglet.

The predicted effect of fitting the pylon/nacelle in the datum position (P1/3), (see Fig. 22) shows clearly the formation of the lower surface shock just inboard of the pylon which dissipates with distance inboard. The associated lower surface suction peak is the prime cause

Copyright © 1998, by the International Council of the Aeronautical Sciences (ICAS)
and the American Institute of Aeronautics and Astronautics, Inc.

of the lift loss on the inboard wing, previously observed in the spanwise lift grading. With a decrease of incidence, the strength of the gully shock increases with further lift loss. Outboard of the pylon, there is a loss of suction on the forward part of the top surface which propagates outboard. This is the feature that causes most of the observed lift loss on the outer wing.

The comparison of predicted and wind tunnel model wing pressures either side of the pylon for the nacelle in each of the 5 positions is shown in Figs 23a to 23e for M = 0.78, $\alpha = 2^{\circ}$. It is significant that the method accurately reflects the total disappearance of the gully shock as the nacelle is moved forward from P1/3 to P1/2. Further study of the comparative plots gives one confidence to suppose that RANSMB has accurately predicted the characteristics of the gully shock. In this respect the CFD method can be used as a design tool and a means to enhance understanding of the aerodynamic sensitivity to the nacelle configuration changes. It will be noticed (Fig. 24a) that the shock at the wing lower surface for the closest nacelle positions (P1/0 and P1/1) looks stronger than for the datum position (P1/3). This was also observed for $\alpha = 1^{\circ}$, and was not reflected as an increase in gully wave drag as noted earlier. A possible reason for this is that the stronger shock is now more confined within the reduced gully flow field. It is interesting that aft of this shock the flow recovers to a more positive pressure for P1/0 than for either P1/1 or P1/3. This effect is partly responsible for the reduced loss of lift for the P1/0 installation.

The effect of moving the nacelle progressively aft from P1/2 through P1/3 to P1/4 (Fig. 24b), again shows the gully shock strength to increase as was observed earlier during the inviscid CFD analysis.

The predicted effect on wing upper and lower surface isobars of adding the pylon/nacelle in the datum position is seen in Fig. 25a to 25d for M = 0.78, $\alpha = 2^{\circ}$, upper surface and $\alpha = 1^{\circ}$ for lower surface.

6 Wing redesign

6.1 Traditional approach

For the wing re-design a number of constraints were prescribed to ensure that the wing remained practicable from an airframe manufacturers' perspective:

1. The wing planform was to remain unaltered.

2. For the wing inboard of the pylon, the section shapes and wing twist could be altered provided that physical thickness at the rear spar was not reduced from the original value.

3. Outboard of the pylon, the wing lower surface could be modified to allow a reasonably smooth blend with the re-designed inner wing, but the upper surface shape was to remain unaltered. However, it was agreed that modification of the outer wing twist should be allowed, in order to achieve the most favourable spanwise lift and wave drag distribution for the nacelle-installed case.

4. The wing was to have a generally smooth and acceptable curvature in both a chordwise and spanwise sense. Between front and rear spars, there would be no significant regions of inflexion and no reduction of available fuel volume (assuming the use of centre-wing tanks).

5. Furthermore, rear spar depth at any spanwise station was not permitted to be reduced from the original value since this would have led to notional difficulties with actuator sizing and trailing-edge flap design.

The design conditions selected were M = 0.78, $C_L = 0.55$ and M = 0.81, $C_L = 0.35$. The latter condition provides the critical case for the wing lower surface design in the region of the pylon.

6.1.1 Wing Re-Design Philosophy

The intention of the design was to achieve a wing, subject to the previously prescribed set of 'design rules', which was effectively desensitised to the effects of nacelle shifts. It had been recognised at an early stage that LDMF nacelle installation needs a great deal of care and attention to avoid the occurrence of gully shocks. To reduce the inboard side constricting effect it was necessary to reduce to a minimum the contraction ratio experienced by the flow in this region. This was achieved by minimising local surface curvatures. The wing lower surface had therefore to be designed in a way which moved the lower surface crest as far aft as could be tolerated. This was to be done while maintaining sufficient rear camber to ensure an acceptable drag rise Mach Number and to avoid the onset of excessive viscous drag. At the same time, the forward part of the lower surface needed to be kept as flat as possible. The blended into the wing leading edge was such that the so-called leading edge chin suction peak was minimised. These sectional characteristics applied at the pylon station had then to be blended spanwise in a way which ensured a wing of low manufacture cost, i.e. by avoiding excessive spanwise curvatures. It had also been recognised that the effect of the nacelle installation was to reduce locally the wing lift. To avoid compromising vortex drag, the wing spanwise lift distribution had therefore to be adjusted to compensate. Finally the twist of the inboard wing relative to the outer wing was adjusted to achieve an acceptable development of wing upper surface shock pattern at the design condition. The

Copyright © 1998, by the International Council of the Aeronautical Sciences (ICAS)
and the American Institute of Aeronautics and Astronautics, Inc.

resulting wing re-design, whilst retaining the upper surface shape outboard of the wing planform kink, had considerable lower surface changes giving rise to a generally reduced front spar depth. Also, a new root section allowed a lower setting angle against the fuselage side. These changes met the design rules and maintained the overall fuel volume.

6.1.2 CFD Results for Re-designed Wing

A comparison of original and re-designed wing section shapes from the root out to the pylon station is shown in Fig. 26. The corresponding pressure distributions either side of the pylon, predicted by RANSMB N-S at M = 0.78, $\alpha = 2^{\circ}$ for the datum nacelle installed case, is shown in Fig. 27. It is seen that the shock inboard of the pylon has been eliminated at this condition. The upper surface pressure distribution on the inner wing is now quite different in character to that shown by the original wing. At $\alpha = 0^{\circ}$, where the lower surface shock inboard of the pylon is stronger, RANSMB indicated a local flow separation on the original wing, whereas the redesigned wing showed no such problem. Comparing drag polars predicted by RANSMB for M=0.78 over the range C_L from 0.3 to 0.55, revealed a drag improvement of a constant 6 to 6.5 drag counts. Similar improvements were seen also at M=0.81.

In the light of the RANSMB results, it was considered that the re-design process had been successful in minimising the adverse effects of nacelle installation.

6.2 Numerical design optimisation

The DERA programme for the Constrained Optimisation Design of Aerodynamic Surfaces (CODAS) has recently become available for use in conjunction with CFD method SAUNA[15]. In order to demonstrate the applicability of the method to complex configurations, the programme was used to optimise the wing with the datum nacelle/pylon. This work was carried out by the Aircraft Research Association (ARA) under contract to DERA.

The basic principle of an optimisation design method such as CODAS is to use a numerical optimisation technique to minimise or maximise some aerodynamic function (e.g. drag), whilst constraining other functions controlling aspects of the geometry such as wing thickness or aerodynamic characteristics such as lift. Numerical optimisation design methods are very powerful because of their ability to handle simultaneously a large number of design variables whilst satisfying necessary constraints on the design. Several design conditions can also be handled simultaneously within the optimisation design, enabling aerodynamic shaping to be chosen for good aerodynamic performance at a variety of operating conditions.

CODAS uses the design cycle shown in Fig 28, coupling an optimisation routine, with the ARA CFD suite SAUNA which provides flow solutions at one or more design points.

The optimiser is a non-linear, gradient-search type, constrained optimisation code. The technique is a recursive two-stage process in which gradient evaluation is followed by a series of search steps. Each design variable is perturbed separately and the effect on the objective and constraint functions is calculated. A complete set of variable perturbations enables the gradient of the objective and constraint functions with respect to each of the design variables to be defined. This gradient information defines a strategy for varying the complete set of variables to reduce the value of objective function, whilst satisfying the constraint functions. Changing some or all of the design variables on the basis of the gradient information then activates the search step stage. The search step may require several separate changes to the values of the variables, with a corresponding evaluation of the design objective and constraint functions for each step. After each successful search step stage, the best design case becomes the baseline for the two-stage gradient-search process to be repeated.

Each gradient-search process constitutes a design cycle (optimisation iteration). Several design cycles are normally required to obtain a converged solution. As the design proceeds, the tolerance controlling how well the constraint functions are satisfied is reduced. Hence, provided the imposed constraints are physically realisable, a solution satisfying the constraints is found at the end of the design process.

The designer is provided with direct control over the objective function and both aerodynamic and geometric constraints by a user-generated subroutine. This allows the user to employ existing function definitions or create functions through FORTRAN programming to build up a library of routines of increasing complexity which can be adapted for each design application. For this exercise a fairly simple programme has been written which aims to satisfy the following criteria:-

- primary design point Mach = 0.78, $C_L = 0.55$.
- high speed design point Mach = 0.81, $C_L = 0.35$.
- pylon and nacelle to remain line-of-flight.
- minimum drag for the fuselage, wing, pylon, nacelle configuration.
- no reduction in wing fuel volume.
- no reduction in front spar depth. .
- no reduction in rear spar depth.

It is possible to specify up to 3 design points in CODAS. The primary design point was used for this design exercise since the introduction of a second design point

Copyright © 1998, by the International Council of the Aeronautical Sciences (ICAS)
and the American Institute of Aeronautics and Astronautics, Inc.

would have doubled the length of each design run. It should also be noted that in this study no allowance has been made for viscous effects, neither through coupled boundary layer calculations nor the addition of a frozen boundary layer displacement thickness, δ^*, to the geometry.

The version of SAUNA available for the flow solver in CODAS was unable to generate a block-structured grid around a pylon that extends beyond the wing trailing edge. Since CODAS requires a completely block structured grid, a simplified pylon was derived from the true geometry by joining the nacelle trailing edge to the wing trailing edge. Maintaining the inboard nacelle/pylon/wing gully area back to the minimum cross sectional area and controlling the expansion of the gully downstream generated the simplified pylon geometry. This preserved the primary wing/pylon/nacelle aerodynamic interference characteristics whilst permitting a SAUNA block-structured grid to be generated. The resulting SAUNA surface grid is shown on Fig. 29.

Fig 30 compares the pressure distributions for a simplified pylon in SAUNA with the true pylon definition using the BAe grid. As would be expected, the differences are greatest in the vicinity of the pylon. However, it is likely that these can be attributed to differences in the grids and their effects on the shocks. The main influence of the pylon modification appears to be a small increase in pressure close to the wing trailing edge.

Since the SAUNA flow solver is used approximately 200 times in a typical CODAS run, the grid must be coarsened to permit realistic run times to be achieved. Fig 31 shows the surface grid and figs 32a-b sections through the field for the coarse grid.

Fig 33 shows a comparison of the wing pressure distribution inboard of the pylon for the coarse and fine grid. The coarse grid predicts the main features of the flow at the design point, although there is some smearing of the shocks, notably the strong shock on the wing lower surface. There is some degradation of the predicted pressure distributions as a result of grid coarsening and remeshing. However, the results from forward runs provide some encouragement that the redesign will be based on a representative estimate of the wing/pylon/nacelle interference.

It is desirable to impose some limits that suggest favourable features or preclude unacceptable solutions from CODAS. For this case a wing upper surface, recompression was imposed at 4 spanwise stations in the vicinity of the pylon, implying a local normal Mach number at the wing leading edge of 1.27, reducing to 1.2 at the shock. A tolerance of 0.05 on the rms. value of the difference between the actual C_p and the target $C_{p_{rec}}$ was also applied which provides a significant amount of flexibility in the level and gradient of the recompression. Since the objective function only optimises the primary design point, a number of aerodynamic constraints have been imposed to reduce the tendency for increased drag at the high-speed design point. The low lift coefficient associated with the high speed design means that the problems occur mainly on the wing lower surface, notably inboard of the pylon. The presence of locally supersonic flow does not cause a major increase in drag because it is concentrated in a small region. However, this does increase the tendency to flow separation in the wing/pylon junction that will result in significant excess drag. This effect would not be predicted by an Euler solution and hence cannot be controlled directly by the objective function. Therefore, the wing lower surface pressures have been controlled by specifying minimum pressures in the vicinity of the pylon and target pressures at spot points inboard of the pylon. It was considered sufficient to impose this constraint at the primary design point since the phenomenon would be similar at the high speed design point.

The geometric constraints were imposed on CODAS by a mathematical expression. The requirement to maintain existing front and rear spar depths was satisfied by locating the position of the spar and calculating the wing thickness at that point for each input control stations. The fuel volume was obtained by calculating the cross sectional area between the spars at each station. The integration of these areas from the body side out to the outer end of the wing box produced the internal volume of the wing as shown on Fig 34.

Three CODAS design runs were carried out, details of which are summarised in Fig 35. In this figure the objective function FUNC(1) (which is the excess drag, total pressure drag less the ideal elliptic lift dependant drag and fuselage pressure drag) is plotted against C_L^2. The line of constant kC_L^2 are lines of constant aerodynamic efficiency and therefore a design change which moves to the right indicates an improvement in aerodynamic efficiency. RUN5 and RUN10 were similar in that they used the same objective function and aerodynamic constraints. RUN10 maintained the existing front and rear spar depths whereas RUN5 allowed the depths to change. Finally, RUN12 used the same objective function and constraints as RUN10, but carried out a design of the pylon rather than the wing.

REDES1 is a combination of the wing from RUN5 with the pylon from RUN12 and it is encouraging to note that the incremental effects of the wing and pylon design changes are approximately additive. This means that CODAS can be used to design the two surfaces independently, giving a saving of total run time. Similarly, REDES2 combines the wing designed to

Copyright © 1998, by the International Council of the Aeronautical Sciences (ICAS)
and the American Institute of Aeronautics and Astronautics, Inc.

RUN10 with the pylon from RUN12.

The redesigned inner wing sections from RUN5 and RUN10 are compared in Figs 36a and 36b. The relaxed geometry constraints of RUN5 have resulted in a more radical modification to the section geometry across the pylon station. Outboard of the pylon there is an increase in section depth and an increase in wing twist. The strict geometric constraint imposed on RUN10 prevents a reduction in spar depth and there is a general increase in section thickness over the inner wing.

The pylon designs for RUN12 are compared on Fig 37. The design has resulted in a toe out setting of approximately 1.8° at the intersection with the wing lower surface with a tendency towards a concave inboard side to the pylon.

The effect of the two redesigns on the pressures on the wing inboard of the pylon is shown in Fig 38 in comparison with the datum configuration. The constrained design, REDES2, shows only minor differences from the datum, whereas the relaxed design REDES1 provides a major weakening of the shock in the vicinity of the pylon. The CODAS redesigns have a similar effect on the wing spanwise distributions, Fig 39. In both cases the loss of lift in the vicinity of the pylon is reduced, resulting in a more closely elliptic spanwise lift distribution.

It has been demonstrated that CODAS can optimise a design whilst retaining control of both the aerodynamic and geometric characteristics of the configuration. The constrained redesign offers a small drag reduction at the primary design point, combined with a 5% increase in inner wing thickness and a 4% increase in wing fuel volume.

8 Conclusions

Comparison of pressure distributions from the 3 methods RANSMB, FLITE3D, SAUNA in inviscid Euler mode have generally shown good agreement for the cases considered. The main differences being ascribed to the treatment of geometry at the wing root and at the wing tip. In particular, for the nacelle installed cases, all methods are in good agreement in resolving the lower surface shock inboard of the pylon. The comparison of absolute drag and of drag changes due to nacelle movement is less satisfactory and possibly highlights the need for a better resolution of the field grid in critical flow regions.

The RANSMB Navier-Stokes code successfully predicts the trends in overall drag due to nacelle vertical and horizontal movement and was even reasonably successful in predicting the magnitude of these drag effects. Considering that the type of nacelle installation under investigation caused the occurrence of a wing lower surface shock inboard of the pylon, this was a particularly pleasing result. Examination of wind tunnel model surface pressure distributions showed that this shock feature was well predicted, especially regarding its ability to show that with nacelle forward movement (to position 2), this shock was eliminated. Furthermore it confirmed that reducing the vertical separation between wing and nacelle was not associated with a drag penalty. This powerful CFD method, when complemented by wind tunnel tests, will allow a better and more detailed understanding of the flow field about complex configurations. This in turn will allow detail design to be carried out to eliminate undesirable flow features.

The DERA constrained optimisation programme CODAS has been used in conjunction with the SAUNA inviscid version CFD code to design a wing/body/pylon/nacelle configuration. The programme has been found to be robust whilst providing the user with freedom to control both aerodynamic and geometric aspects of the design. The results show that the programme gives an improved design according to the objective function which is being optimised, subject to the aerodynamic and geometric constraints which are imposed on the problem.

7 Future Work

The wing re-design exercise described was restricted mainly to making the wing lower surface more tolerant to a closely-coupled LDMF installation. However, the Navier-Stokes CFD work showed that the effect on the wing upper surface was equally as important in its effect, especially on wave drag. The work on the optimisation methodology, CODAS, described in this paper has shown its capability within the set design parameters and suggests itself as the most suitable tool for the design of the wing upper surface, with an installed nacelle. Its perceived value lies in the ability to allow one to constrain wing geometry to within manufacturing limits (for example in terms of spar depth and particularly spanwise smoothness) whilst achieving an optimum aerodynamic performance. Future work will therefore include an attempt to use CODAS with an allowance for viscous effects to improve the previously described re-designed wing upper surface, with consideration being given to manufacture a wind tunnel model at a later date.

9 Acknowledgements

The authors wish to acknowledge Mr D. Stanniland of ARA for his work on the application of CODAS to civil transport wings with underwing mounted engines and Mr J. Doherty, DERA for software support. Also, the authors wish to thank Mr G. Hargreaves, BAe and Mr A. Shires, DERA for assistance and providing material during the preparation of this paper. This work has been carried out with the joint support of the British Department of Trade and Industry.

Copyright © 1998, by the International Council of the Aeronautical Sciences (ICAS)
and the American Institute of Aeronautics and Astronautics, Inc.

"All rights reserved © Copyright 1998, DERA(Crown) and BRITISH AEROSPACE PLC. The Copyright in this paper belongs jointly to DERA(Crown) and to BRITISH AEROSPACE PLC, who are agreeable to the reproduction of the paper in the ICAS 1998 proceedings."

References

1. J.T.Kutney Advancements in aerodynamic integration of engine and airframe systems for subsonic aircraft. INT.J.TURBO & JET ENGINES 1983-84.
2. J.T.Kutney Pylon for aircraft turbo-fan US Patent 4314681.
3. F.B.Ogilvie, A.E.Harris Underwing engine installation for aircraft GB 2144688-B
4. K.C.Hackett, M.R.Schofield. Aircraft wing pylon extensions for minimised aerodynamic penalties US Patent 5,102,069, GB8928038, EP90313338.7
5. C.C.Rossow, H.Hoheisel Numerical study of interference of wing mounted advanced engine concepts. ICAS-94-6.4.1
6. C.C.Rossow, A.Ronzhelmer Investigation of interference phenomena of modern wing-mounted high-bypass-ratio engines by the solution of the Euler-equations AGARD-CP-498
7. F.T.Lynch Modern role of CFD in addressing airframe/engine integration issues for subsonic transports ICAS 94-6.4.3
8. J.J. Benton Description of Methods used by British Aerospace. Notes on Numerical Fluid Mechanics Vol42, Euroval - An European Initiative on Validation of CFD Codes 1990-1992
9. W. Haase, E.Chaput, E.Elsholtz, M. Leschziner, U Mueller ECARP - Validation of CFD Codes and Assessment of Turbulence Models. Notes on Numerical Fluid Mechanics Vol 58 Vieweg 1997
10. G.Kalitzin, A.R.N.Gould, J.J.Benton Application of Two-Equation Turbulence Models in Aircraft Design AIAA 96-0327, January 15-18, 1996/Reno, NV
11. O.Hassan, K.Morgan, J.Peraire An Implicit Finite Element Method for High Speed Flows AIAA 90-0402
12. K.Morgan, J.Peraire, J.Peirot Unstructured Grid Method for Compressible AGARD-R-787 No. 5, May 1992
13. J.A.Shaw, J.M.Georgala, P.N.Childs, C.A.McHugh, N.E.May, A.J.Peace Validation and Evaluation of the Advanced Aeronautical CFD System SAUNA - A Method Developers View. Paper 3, European Forum on Recent Developments and Applications in Aeronautical CFD September 1993
14. G.Kalitzin, A.R.B.Gould, J.J.Benton Application of two-equation turbulence models in aircraft design AIAA 96-0237
15. D.A.Lovell, J.J.Doherty Aerodynamic design of aerofoils and wings using a constrained optimisation method ICAS 95-2.1.2

Table 1 - Wing/Body (Inviscid) Methods Comparison, M=0.78

Method	a=1°		a=2°	
	C_L	C_D	C_L	C_D
RANSMB	0.4768	0.01119	0.6199	0.01903
FLITE3D	0.4802	0.0034	0.6232	0.01084
SAUNA			0.6108	0.01751
SAUNA /BAe grid			0.5966	0.01946

Table 2 - Wing/Body/Pylon/Nacelle Configuration (Inviscid), M=0.78, a=1°

Method	Pos. P1/2		Pos. P1/3		Pos. P1/4	
	C_L	C_D	C_L	C_D	C_L	C_D
RANSMB	0.4530	0.01145	0.4439	0.01170	0.4370	0.01191
FLITE3D	0.4634	0.00333	0.4507	0.00343	0.4448	0.00308
SAUNA	0.4457	0.01123	0.4321	0.01138	0.4319	0.01139

Table 3 - Wing/Body/Pylon/Nacelle Configuration (Inviscid) Change in Forces due to Nacelle Shift (Relative to P1/3), M=0.78, a=1°

Method	P1/2-P1/3			P1/4-P1/3		
	ΔC_L	ΔC_D	ΔC_{DI}	ΔC_L	ΔC_D	ΔC_{DI}
RANSMB	0.0091	-0.00025	-0.00054	-0.0069	0.00021	0.00042
FLITE3D	0.0127	-0.00010	-0.00051	-0.0059	-0.00035	-0.00016
SAUNA	0.0136	-0.00015	-0.00058	-0.0002	0.00001	0.00001

Table 4 - Model M2379 Reference Dimensions

Wing Area (S)	4.3229ft²
Semi-Span (b/2)	4.40425ft
Geometric mean chord	0.9815ft
Quarter chord sweep	28°
Aspect Ratio	8.974

Table 5 Variation of Wave Drag with Nacelle Position - RANSMB (Navier-Stokes), M=0.78, Re=4.1x10⁶./ft

Nacelle Position	a=1°			a=2°		
	C_L	$C_{D(wave)L/S}$	$C_{D(wave)U/S}$	C_L	$C_{D(wave)L/S}$	$C_{D(wave)U/S}$
P1/0	0.3982	1.27	3.09	0.5304	0.25	16.32
P1/1	0.3956	1.61	3.02	0.5269	0.25	16.40
P1/2	0.3993	0.14	2.26	0.5316	0.0	15.12
P1/3	0.3890	1.68	3.03	0.5226	0.16	16.24
P1/4	0.3852	2.97	3.54	0.5151	0.85	17.01
Nacelle off	0.4070	0	1.51	0.5348	0	16.44

Drag coefficients quoted in counts, i.e. CD x104.
U/S denotes Wing Upper Surface, L/S denotes Wing Lower Surface

Copyright © 1998, by the International Council of the Aeronautical Sciences (ICAS)
and the American Institute of Aeronautics and Astronautics, Inc.

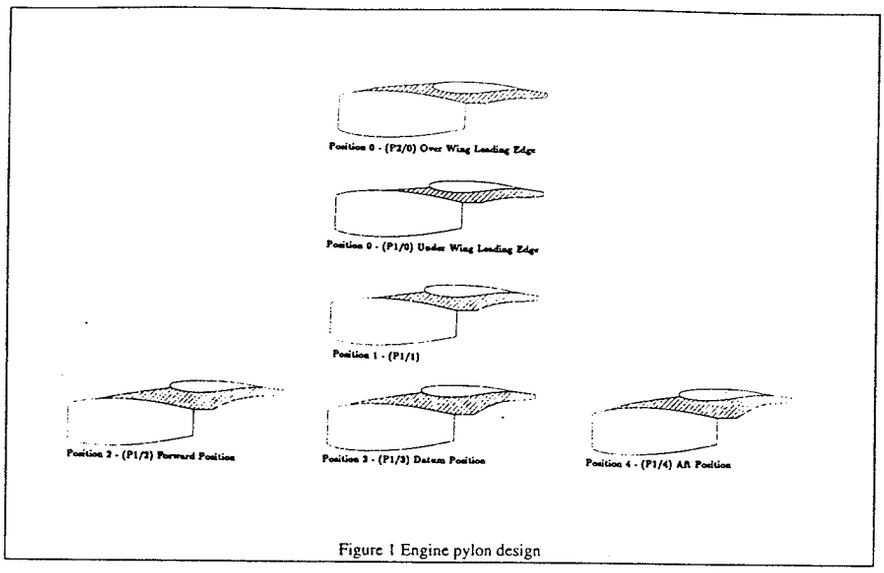

Figure 1 Engine pylon design

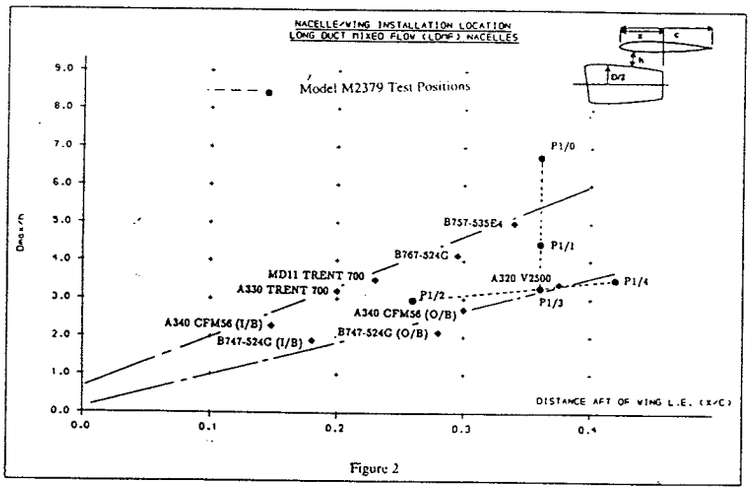

Figure 2

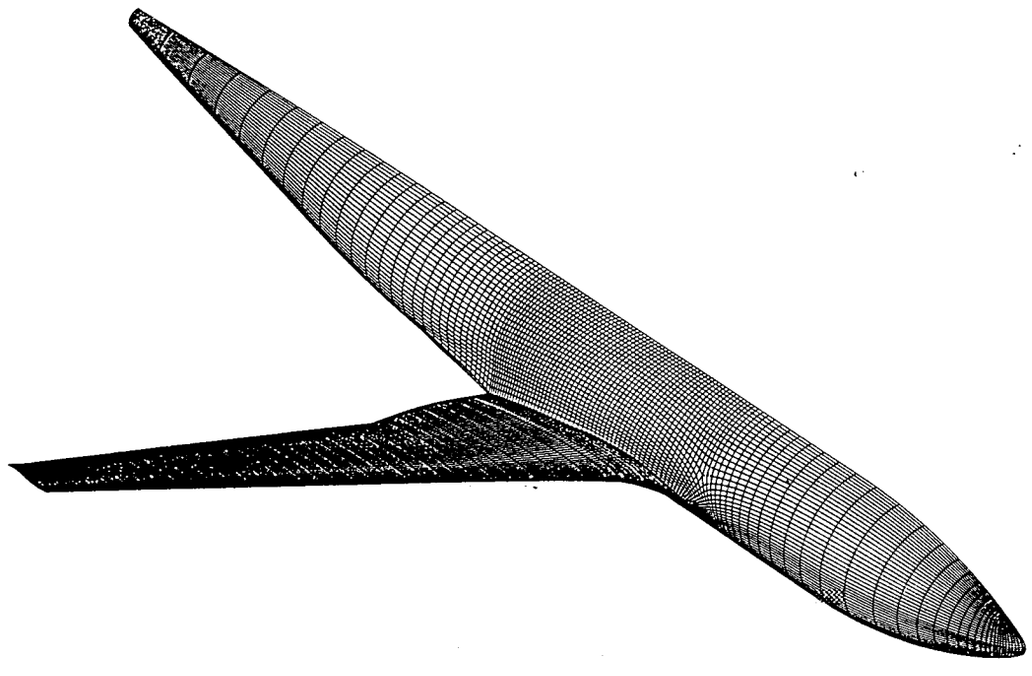

Figure 3 SAUNA surface grids on the wing/fuselage alone configuration

Copyright © 1998, by the International Council of the Aeronautical Sciences (ICAS)
and the American Institute of Aeronautics and Astronautics, Inc.

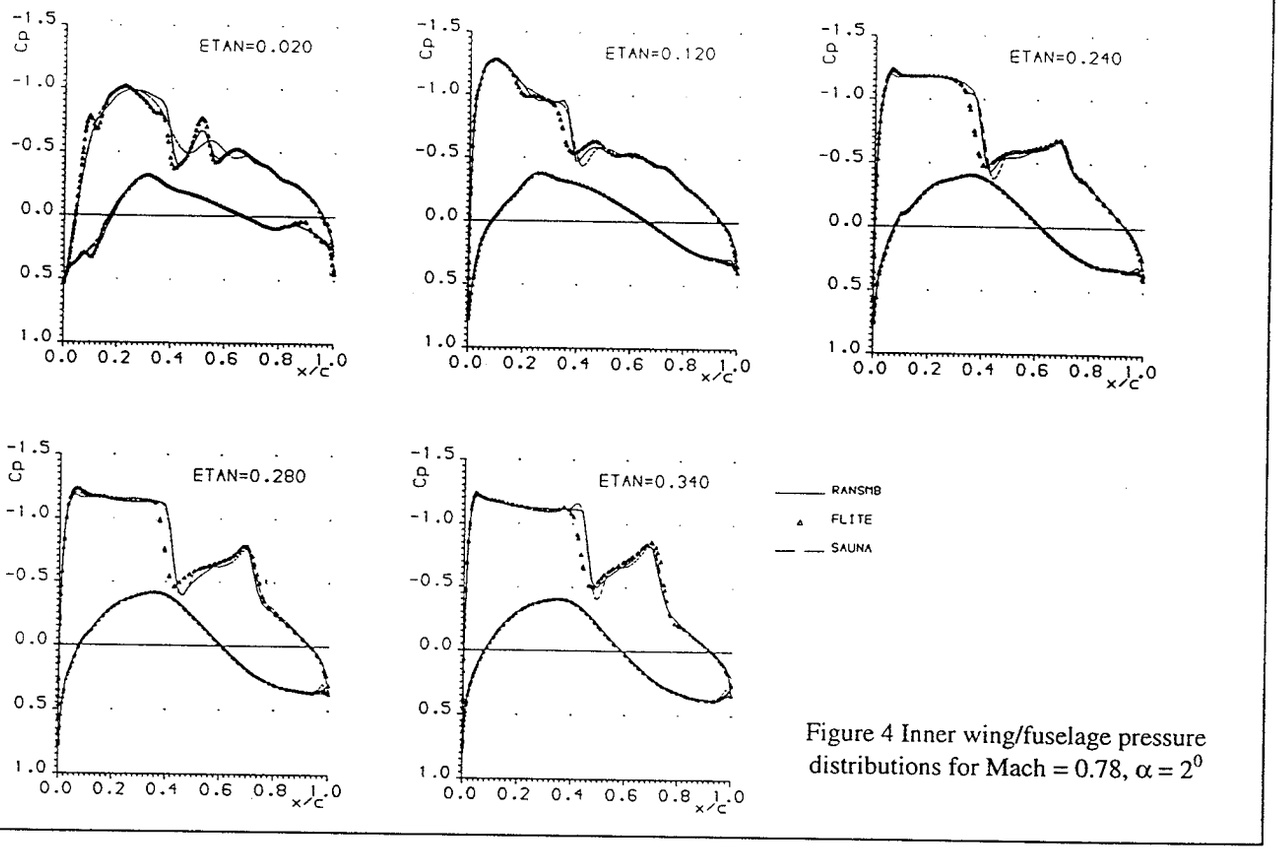

Figure 4 Inner wing/fuselage pressure distributions for Mach = 0.78, $\alpha = 2^0$

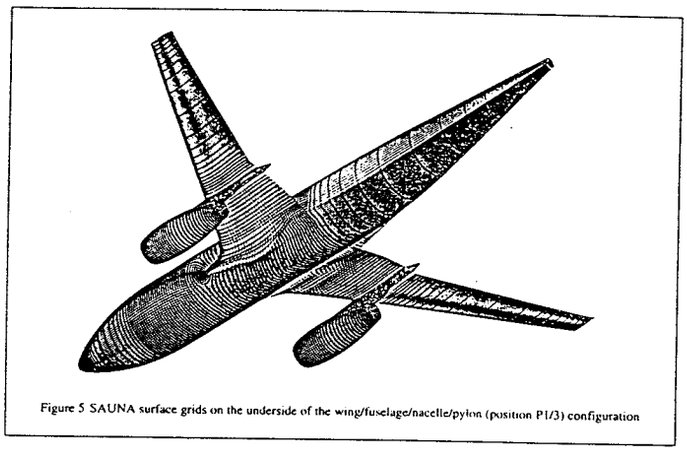

Figure 5 SAUNA surface grids on the underside of the wing/fuselage/nacelle/pylon (position P1/3) configuration

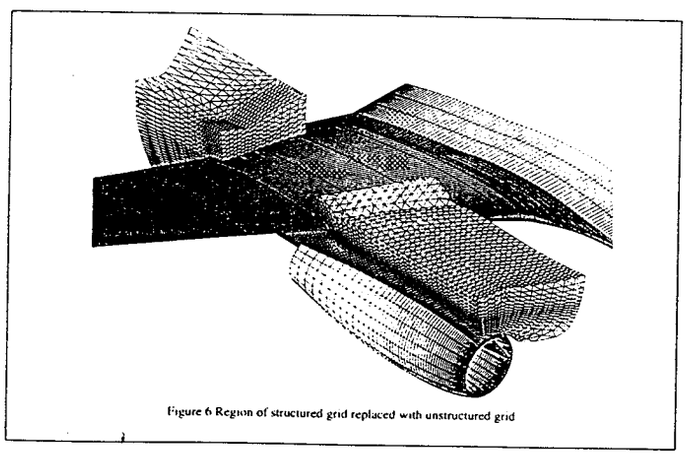

Figure 6 Region of structured grid replaced with unstructured grid

Copyright © 1998, by the International Council of the Aeronautical Sciences (ICAS)
and the American Institute of Aeronautics and Astronautics, Inc.

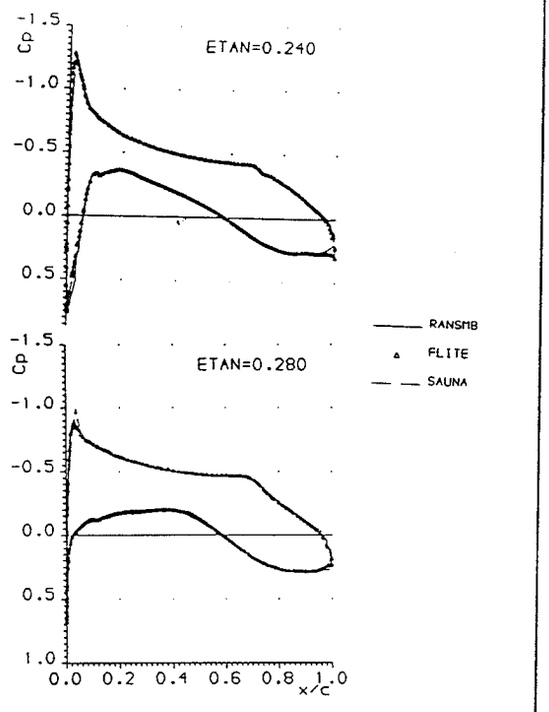

Figure 7 Wing/fuselage/nacelle/pylon pressure distributions for position P1/3, Mach =0.5, $\alpha = 2°$

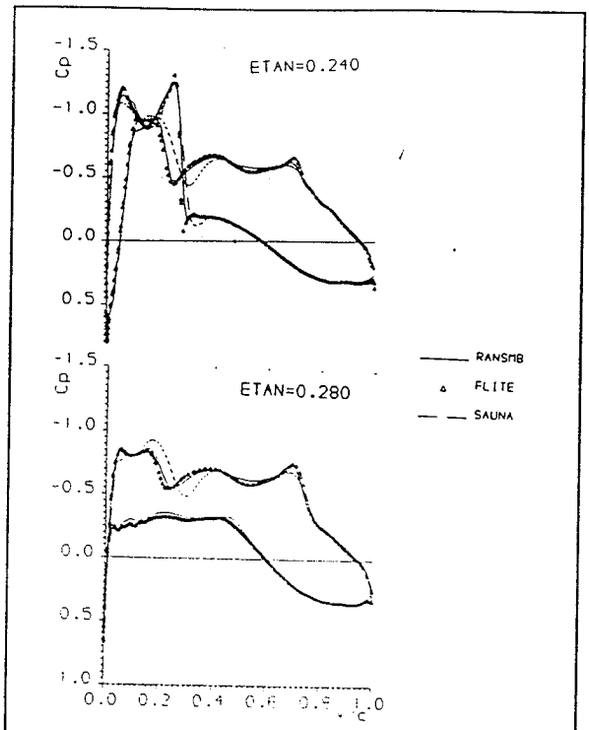

Figure 8 Wing/fuselage/nacelle/pylon pressure distributions for position P1/3, Mach =0.78, $\alpha = 1°$

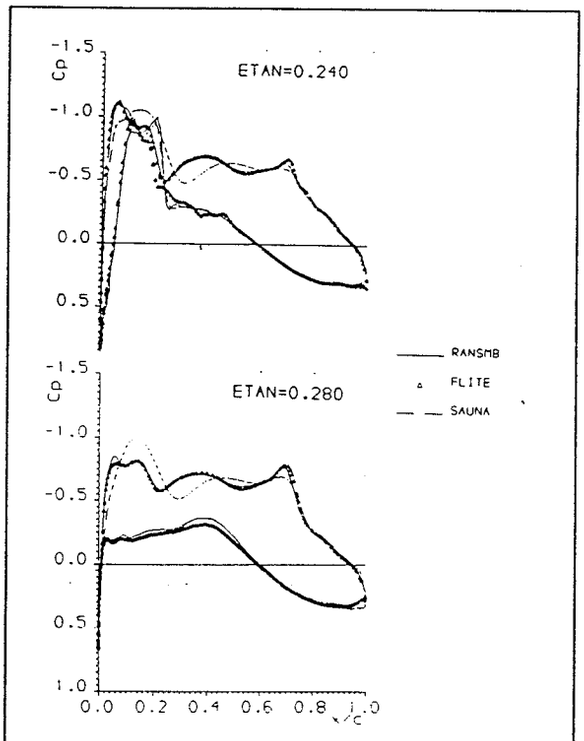

Figure 9a Wing/fuselage/nacelle/pylon pressure distributions for position P1/2, Mach =0.78, $\alpha = 1°$

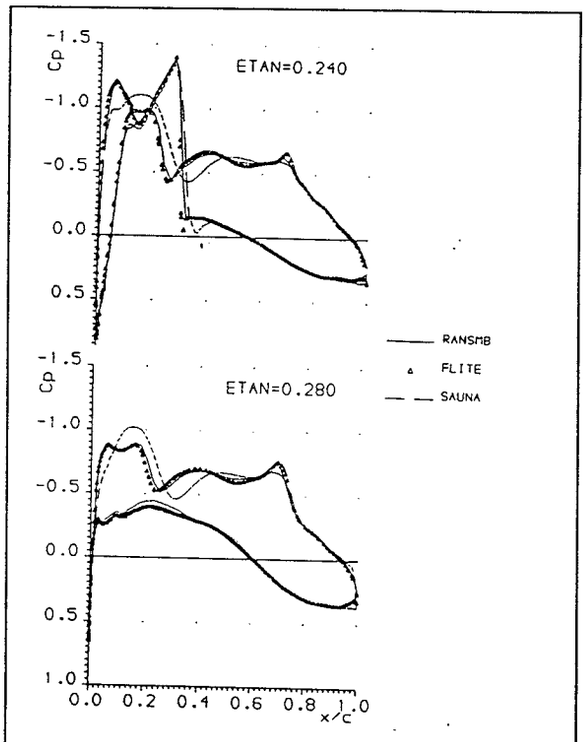

Figure 9b Wing/fuselage/nacelle/pylon pressure distributions for position P1/4, Mach =0.78, $\alpha = 1°$

Copyright © 1998, by the International Council of the Aeronautical Sciences (ICAS)
and the American Institute of Aeronautics and Astronautics, Inc.

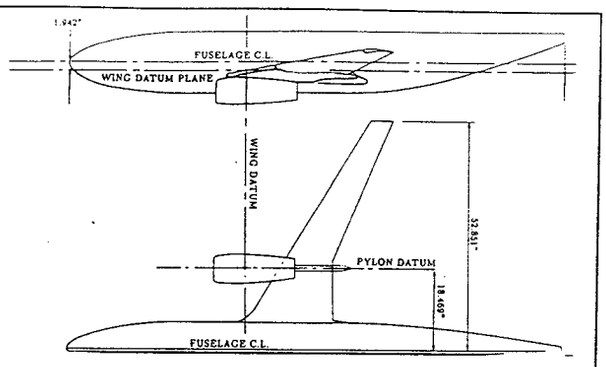

Figure 10 Model Installation

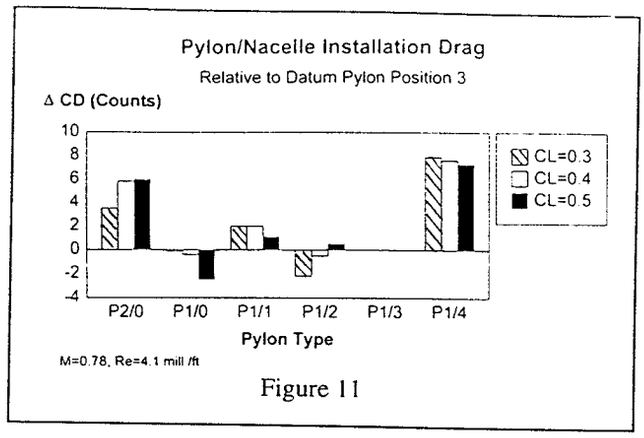

Figure 11

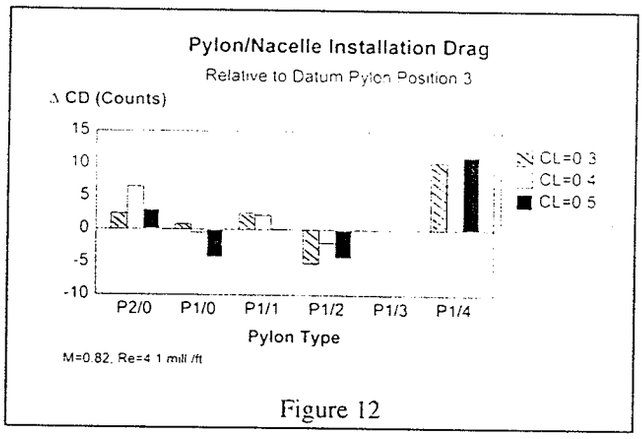

Figure 12

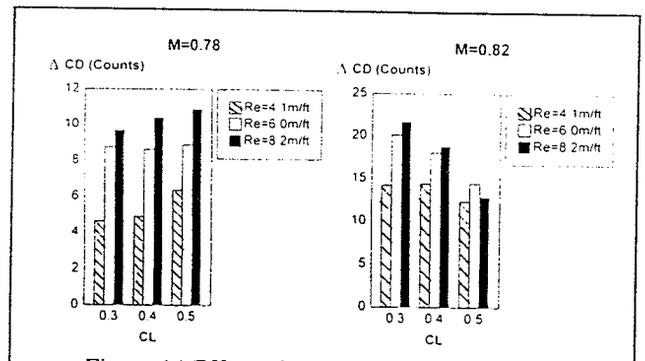

Figure 14 Effect of Reynold number variation on interference drag

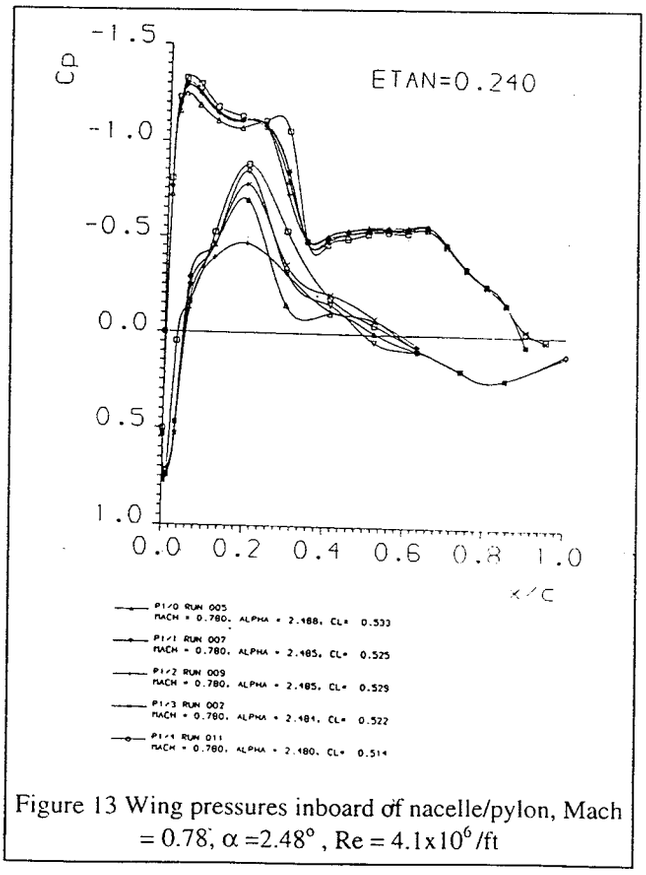

Figure 13 Wing pressures inboard of nacelle/pylon, Mach = 0.78, α =2.48°, Re = 4.1x10^6/ft

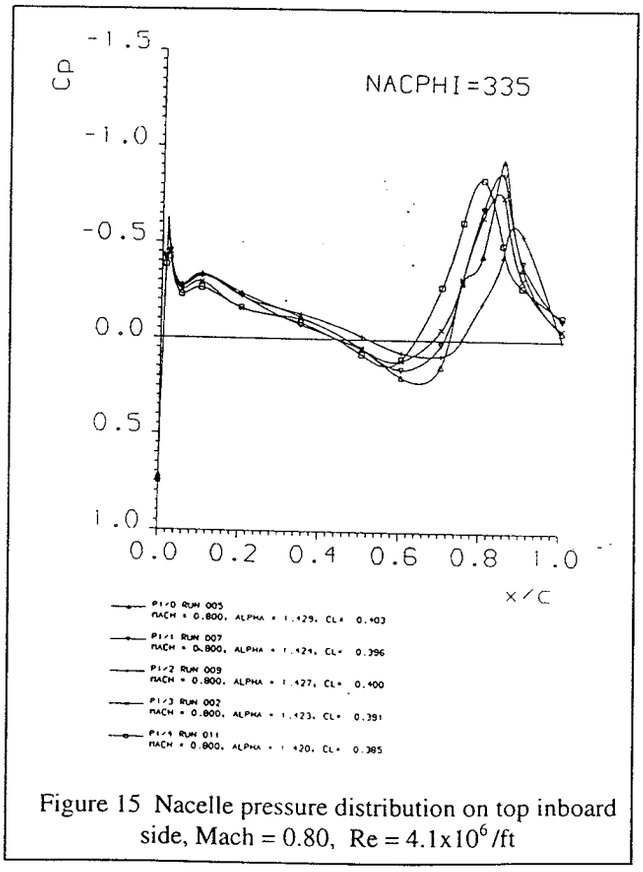

Figure 15 Nacelle pressure distribution on top inboard side, Mach = 0.80, Re = 4.1x10^6/ft

Copyright © 1998, by the International Council of the Aeronautical Sciences (ICAS)
and the American Institute of Aeronautics and Astronautics, Inc.

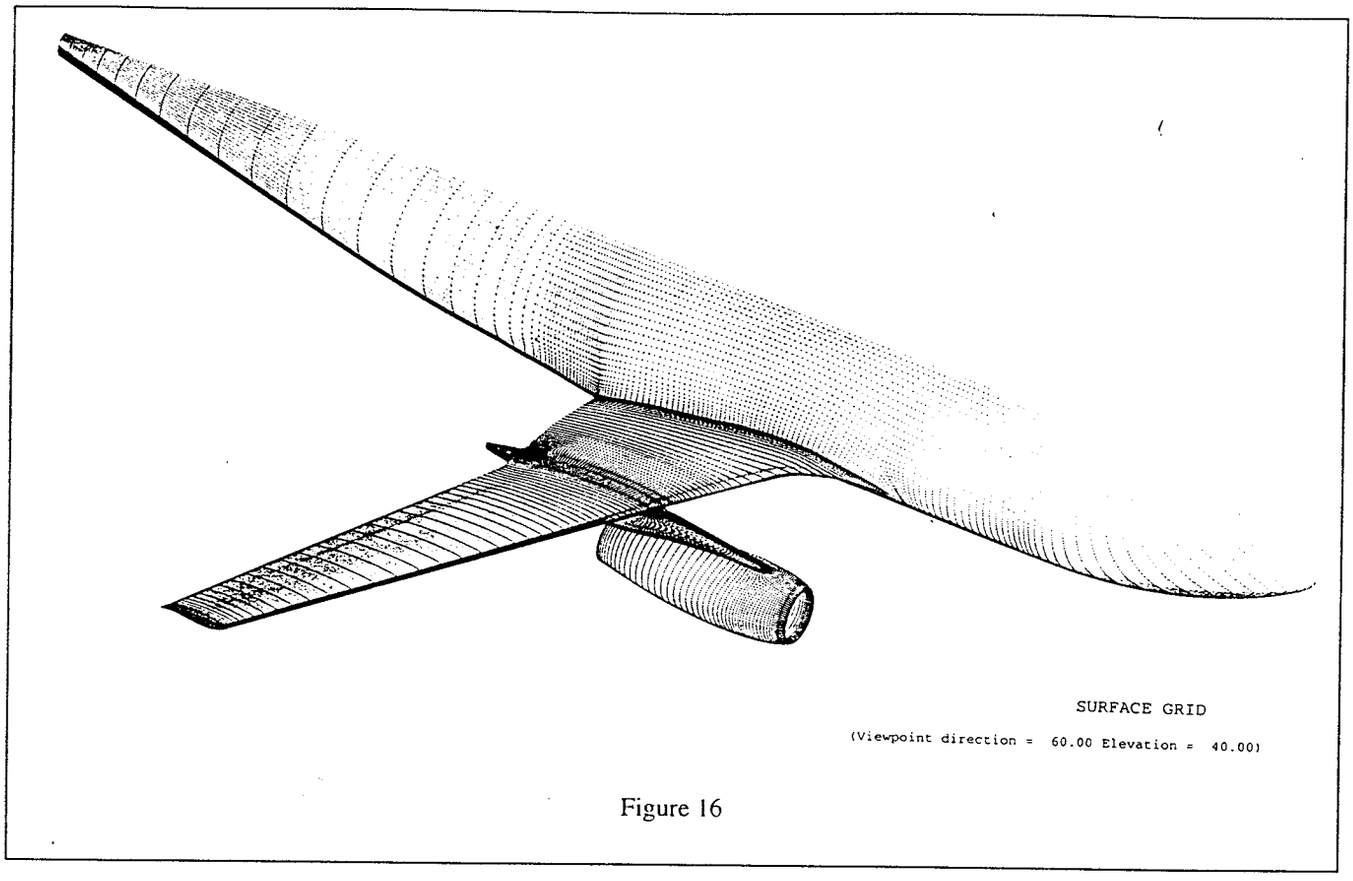

Figure 16

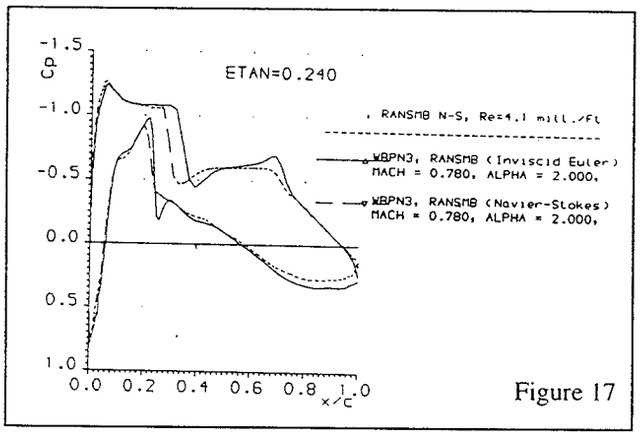

Figure 17

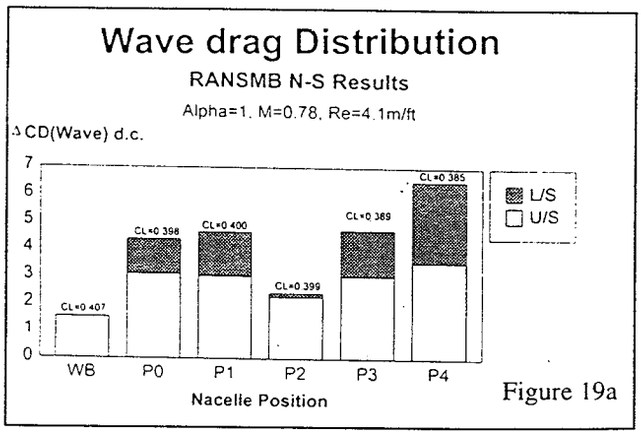

Figure 19a

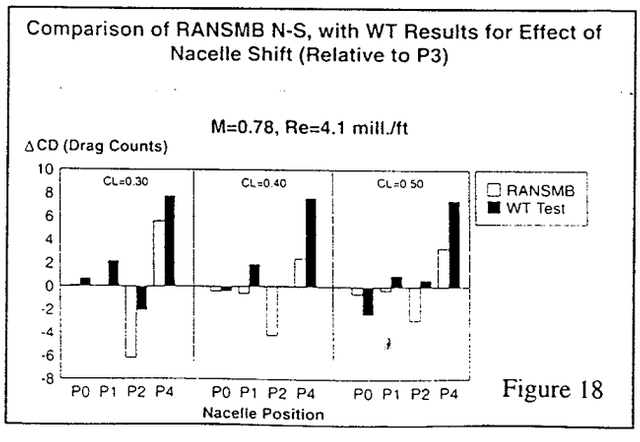

Figure 18

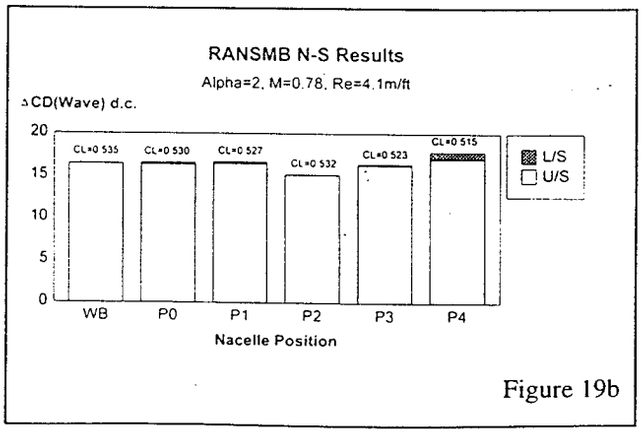

Figure 19b

Copyright © 1998, by the International Council of the Aeronautical Sciences (ICAS)
and the American Institute of Aeronautics and Astronautics, Inc.

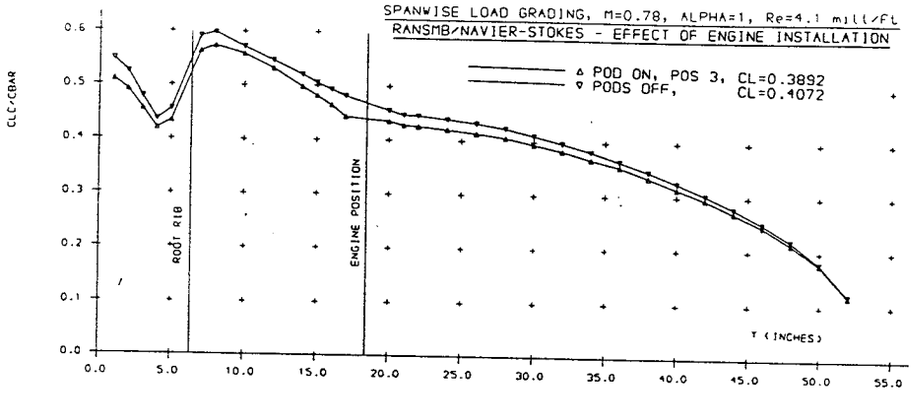

Figure 20a Effect of nacelle at position P1/3

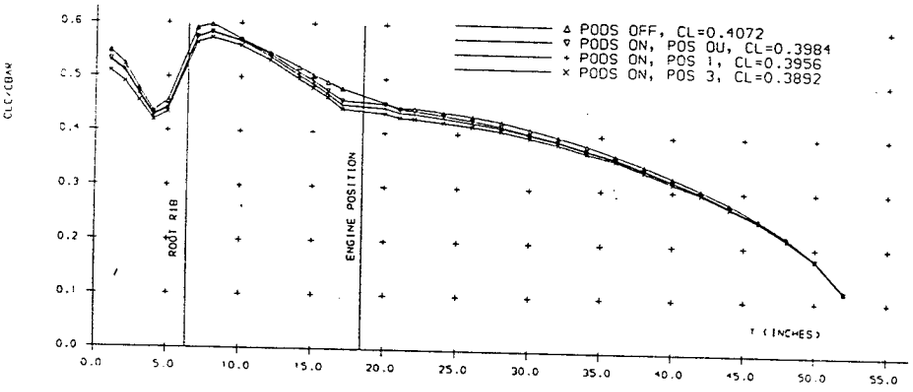

Figure 20b Effect of nacelle vertical movement

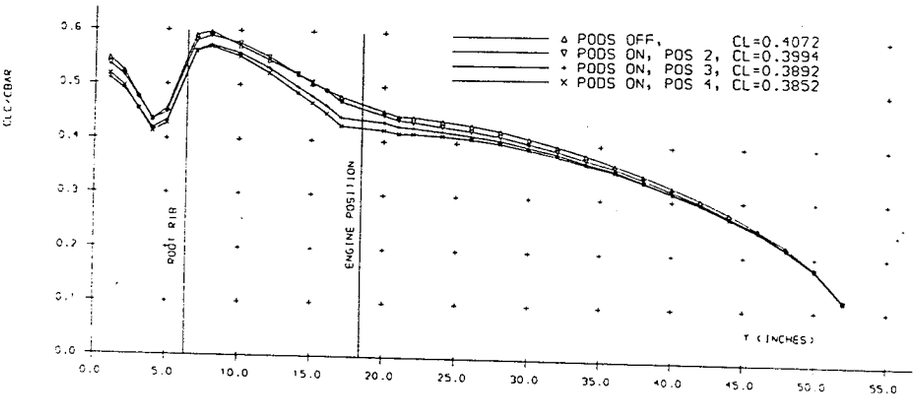

Figure 20c Effect of nacelle forward/aft movement

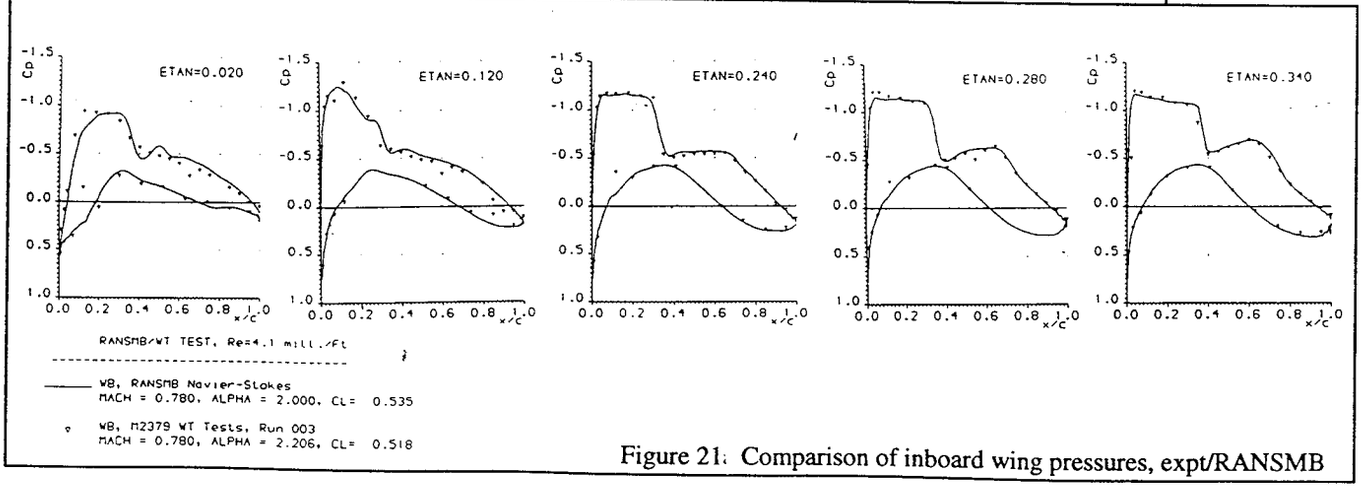

Figure 21: Comparison of inboard wing pressures, expt/RANSMB

Copyright © 1998, by the International Council of the Aeronautical Sciences (ICAS)
and the American Institute of Aeronautics and Astronautics, Inc.

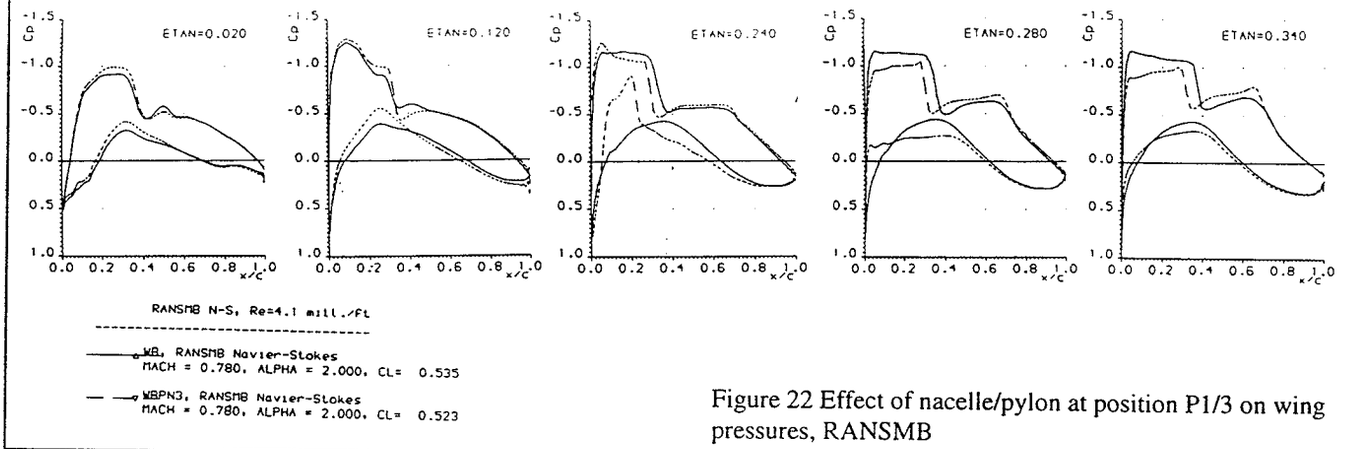

Figure 22 Effect of nacelle/pylon at position P1/3 on wing pressures, RANSMB

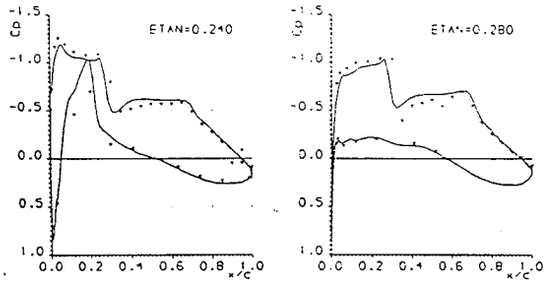

(a) Nacelle/pylon position P1/0

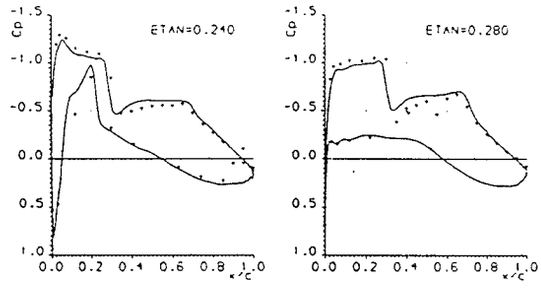

(b) Nacelle/pylon position P1/1

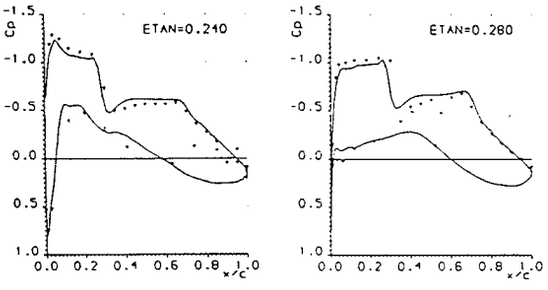

(c) Nacelle/pylon position P1/2

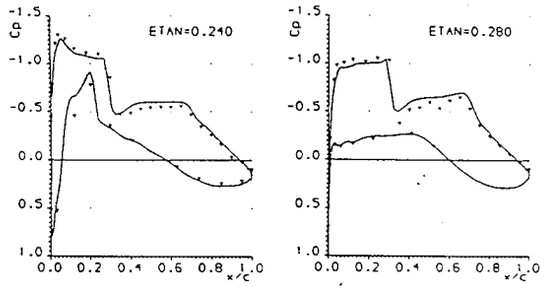

(d) Nacelle/pylon position P1/3

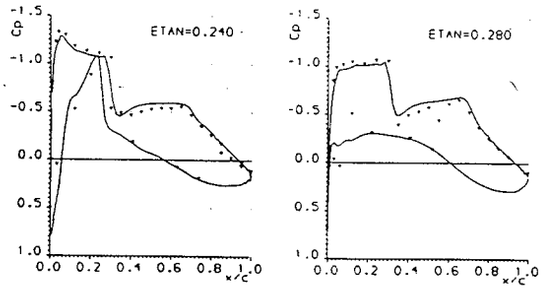

(e) Nacelle/pylon position P1/4

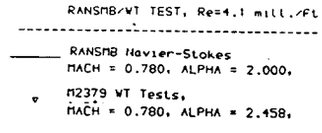

Figure 23 Comparison of wing pressures near nacelle/pylon, expt/RANSMB

Copyright © 1998, by the International Council of the Aeronautical Sciences (ICAS)
and the American Institute of Aeronautics and Astronautics, Inc.

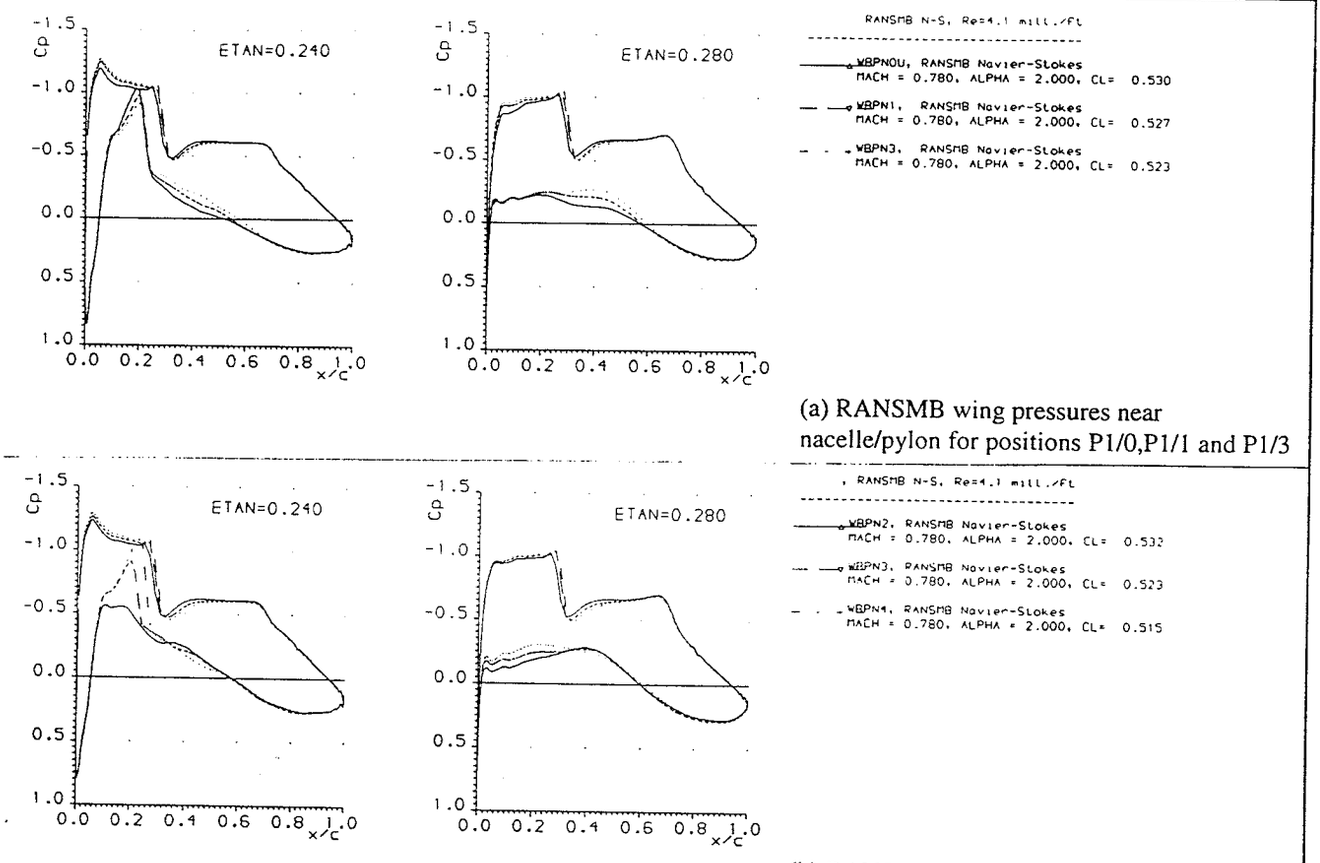

(a) RANSMB wing pressures near nacelle/pylon for positions P1/0,P1/1 and P1/3

(b) RANSMB wing pressures near nacelle/pylon for positions P1/2,P1/3 and P1/4

Figure 24

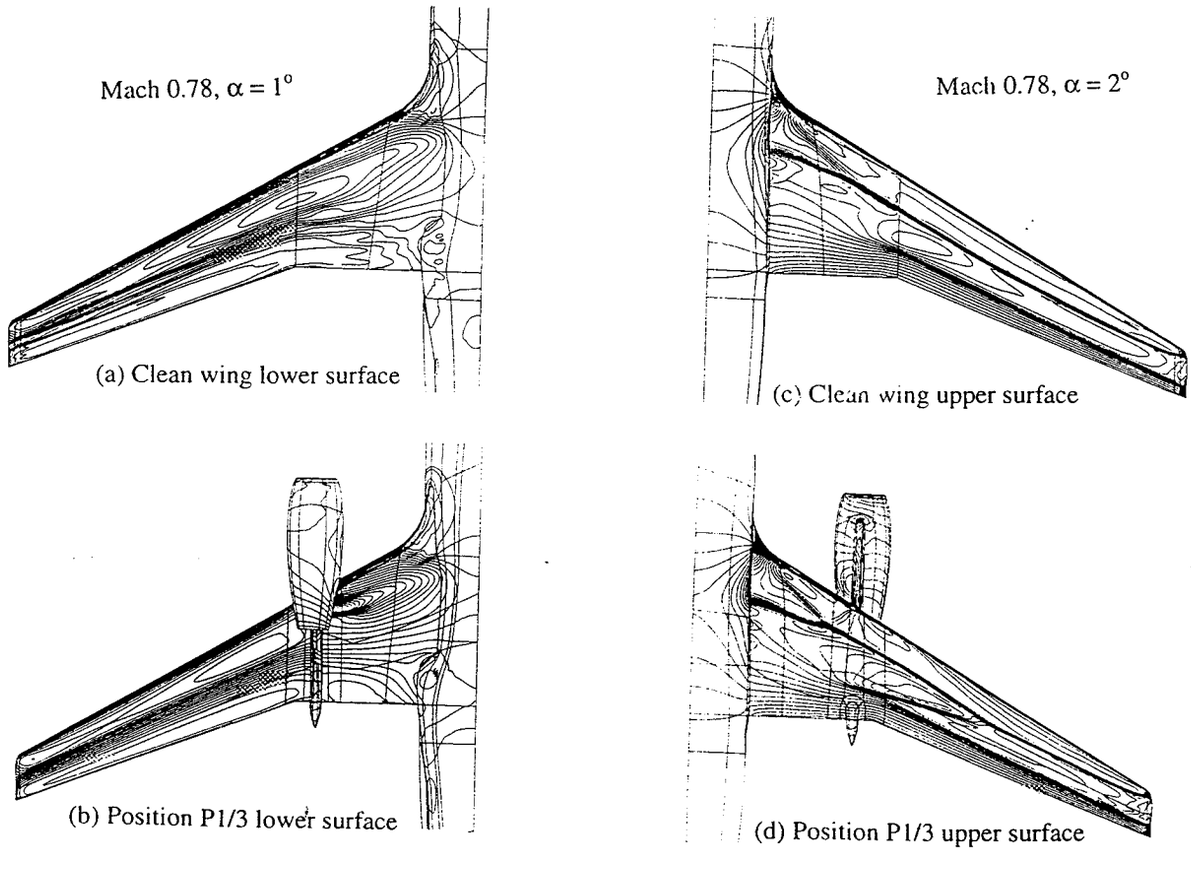

(a) Clean wing lower surface

(c) Clean wing upper surface

(b) Position P1/3 lower surface

(d) Position P1/3 upper surface

Figure 25 RANSMB wing upper and lower surface isobars

Copyright © 1998, by the International Council of the Aeronautical Sciences (ICAS)
and the American Institute of Aeronautics and Astronautics, Inc.

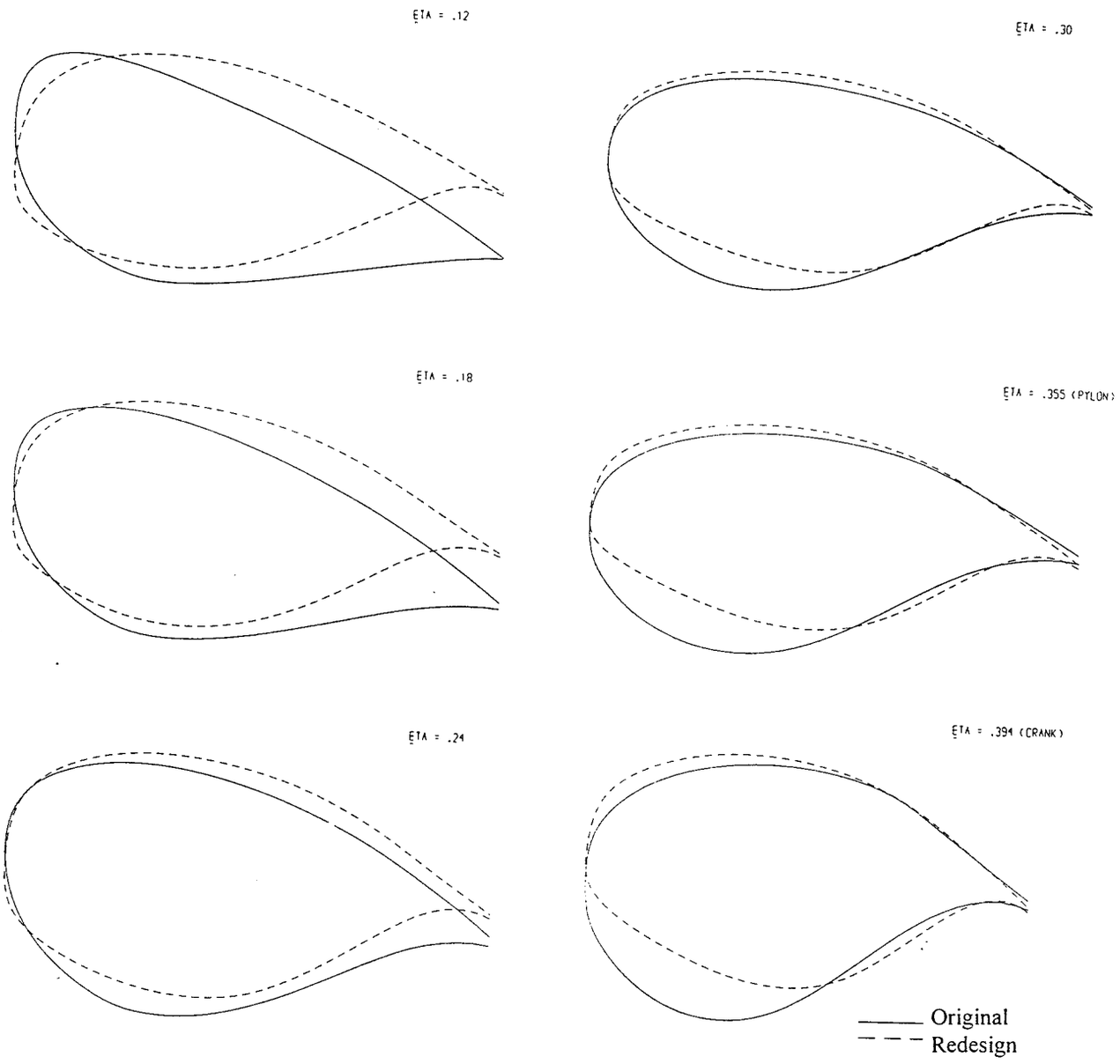

Figure 26 Comparison of original (M2379) and redesigned wing section shapes

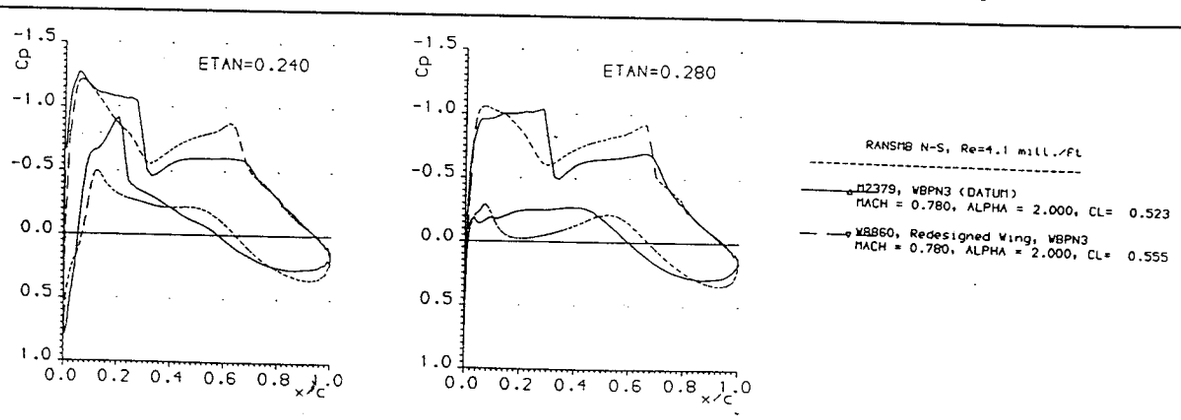

Figure 27 Comparison of original (M2379) and redesigned wing pressures near nacelle/pylon, position P1/3

Copyright © 1998, by the International Council of the Aeronautical Sciences (ICAS)
and the American Institute of Aeronautics and Astronautics, Inc.

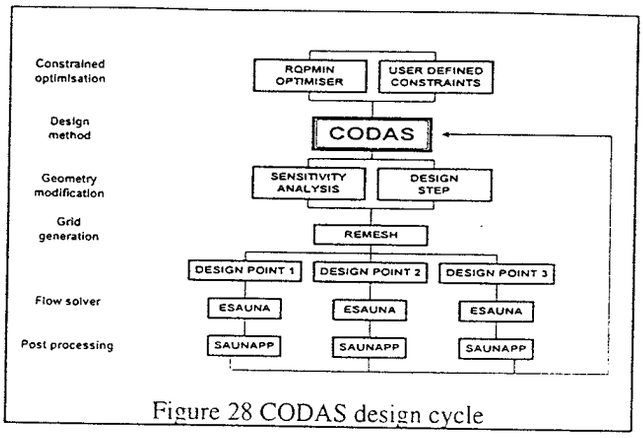

Figure 28 CODAS design cycle

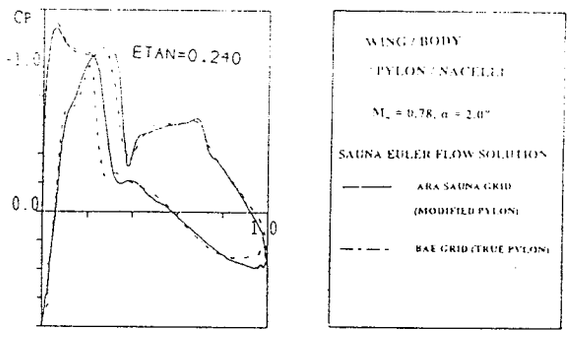

Figure 30 SAUNA pressure distribution comparison true/simple pylon

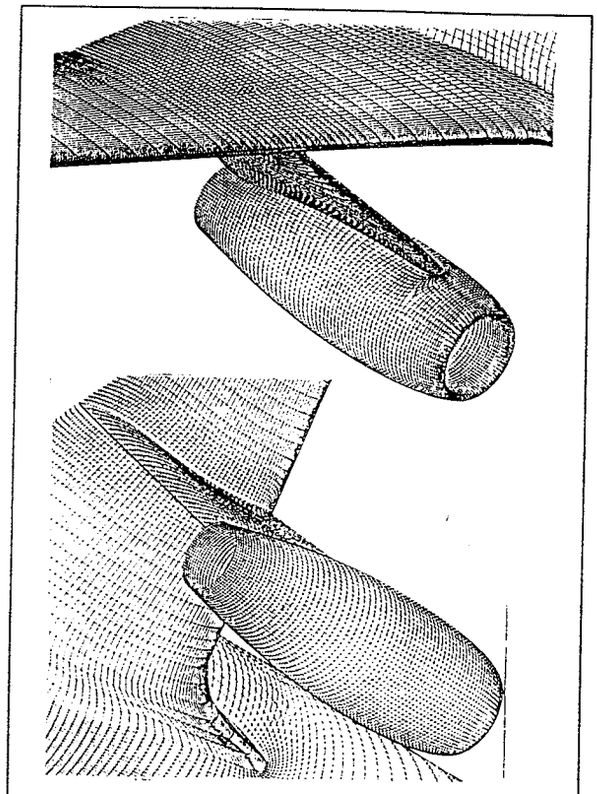
Figure 29 SAUNA surface grids with simple pylon

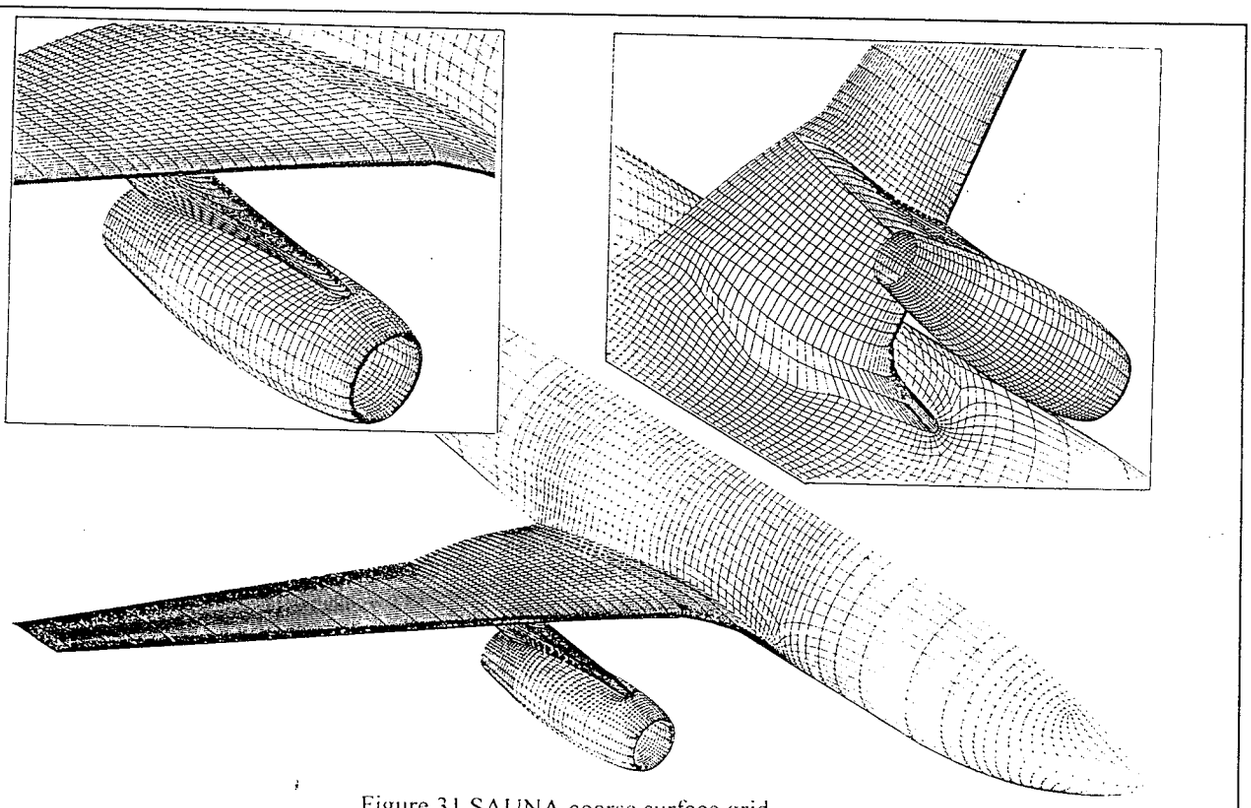
Figure 31 SAUNA coarse surface grid

Copyright © 1998, by the International Council of the Aeronautical Sciences (ICAS)
and the American Institute of Aeronautics and Astronautics, Inc.

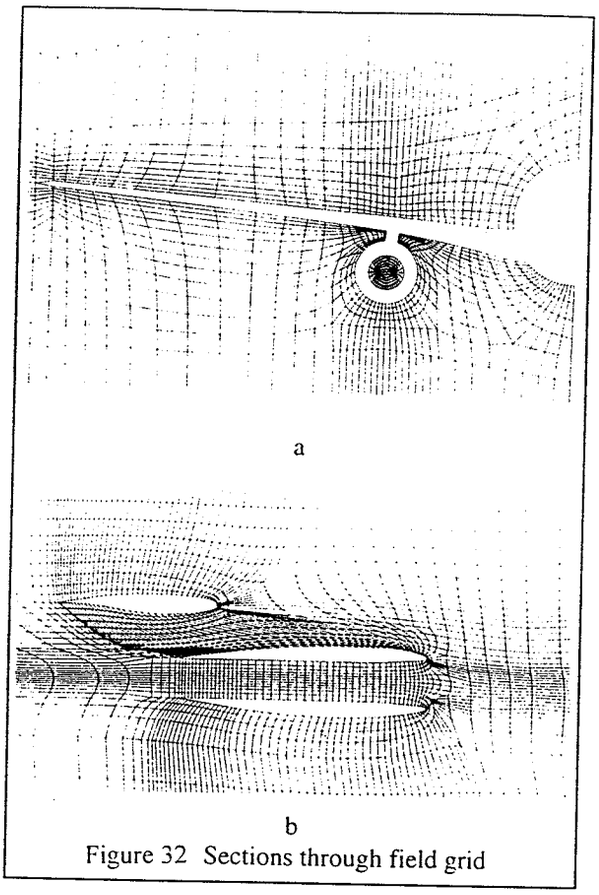

Figure 32 Sections through field grid

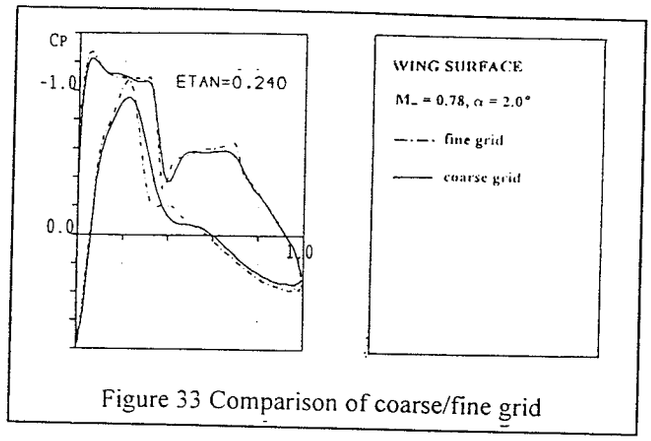

Figure 33 Comparison of coarse/fine grid

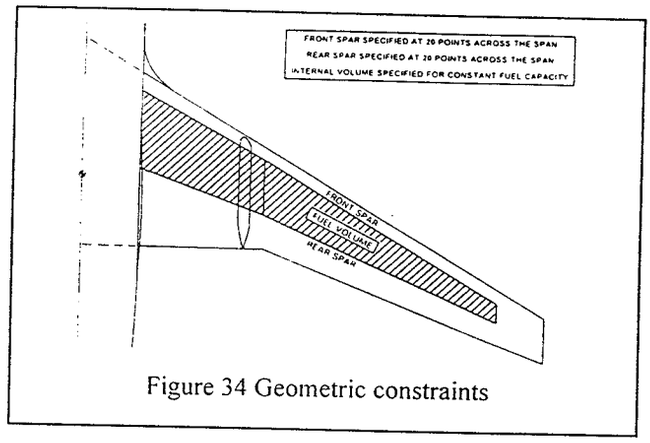

Figure 34 Geometric constraints

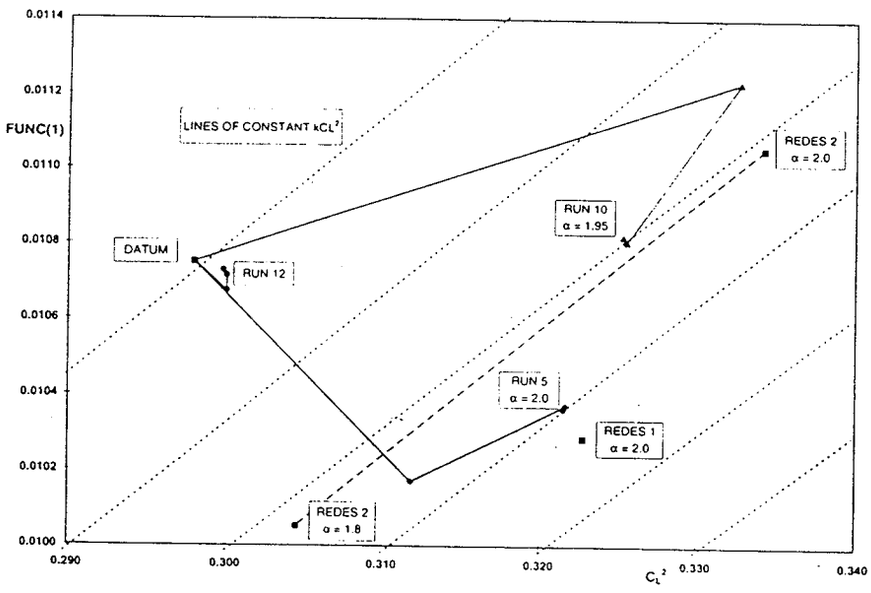

Figure 35 Wing/pylon design optimisation using CODAS

Copyright © 1998, by the International Council of the Aeronautical Sciences (ICAS)
and the American Institute of Aeronautics and Astronautics, Inc.

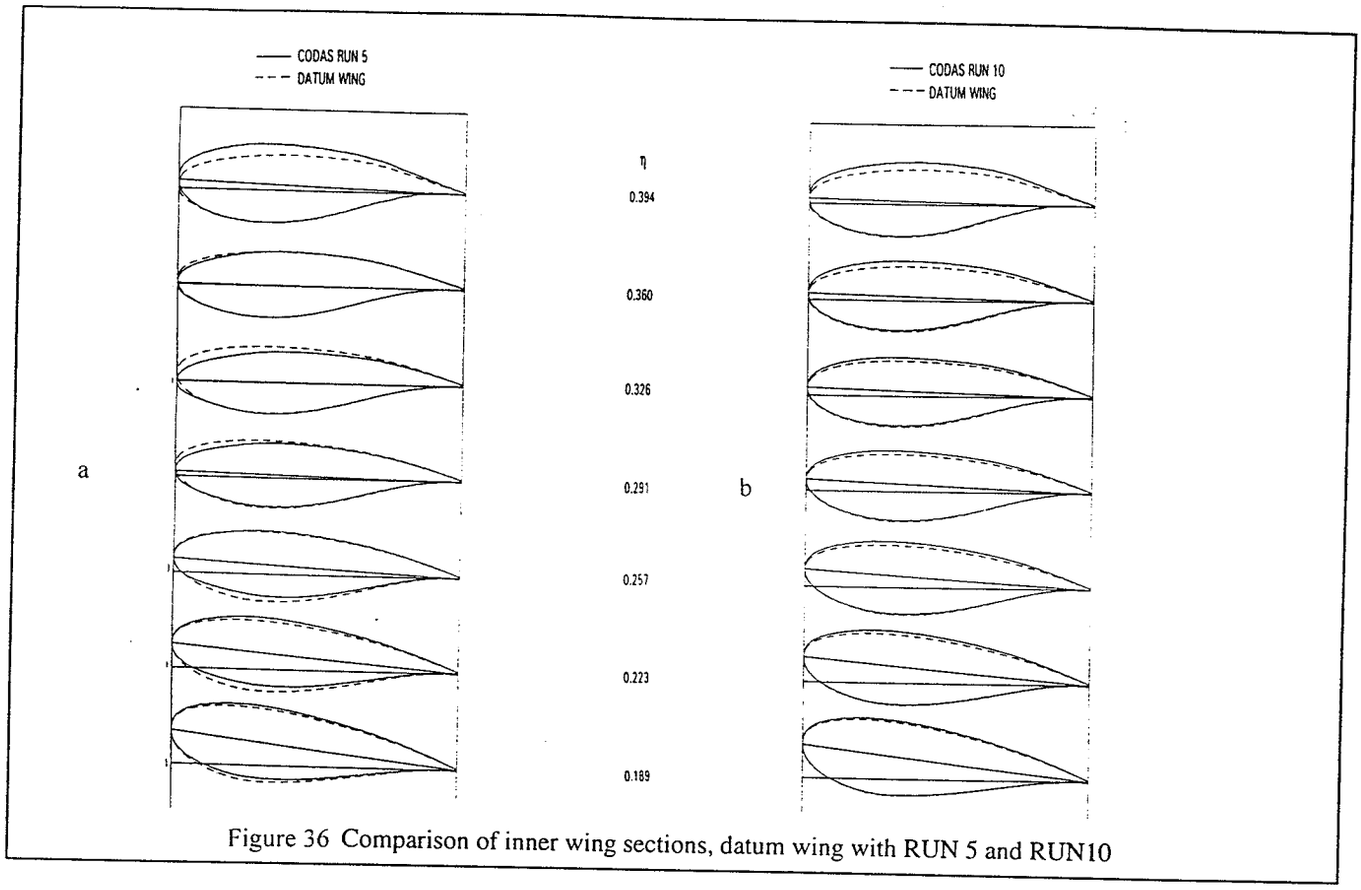

Figure 36 Comparison of inner wing sections, datum wing with RUN 5 and RUN10

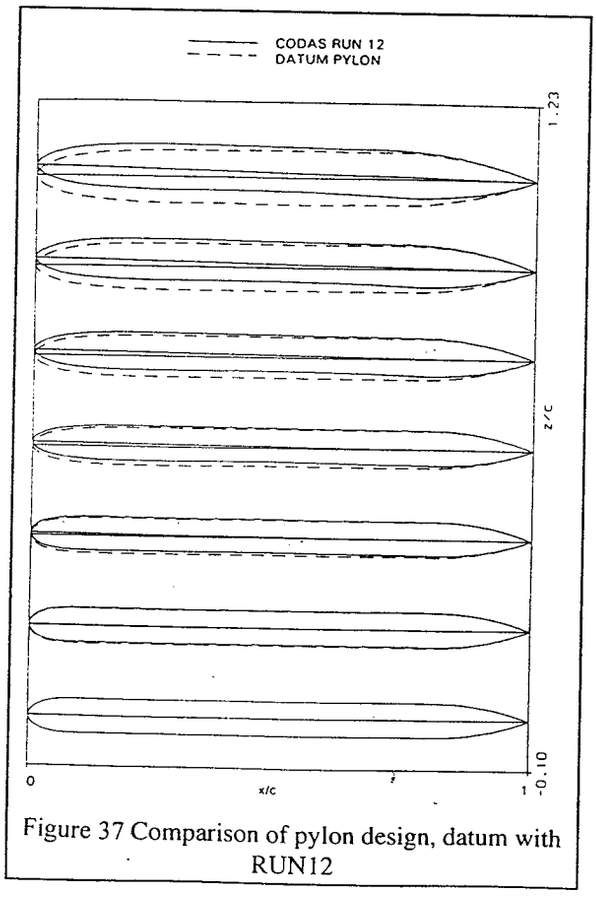

Figure 37 Comparison of pylon design, datum with RUN12

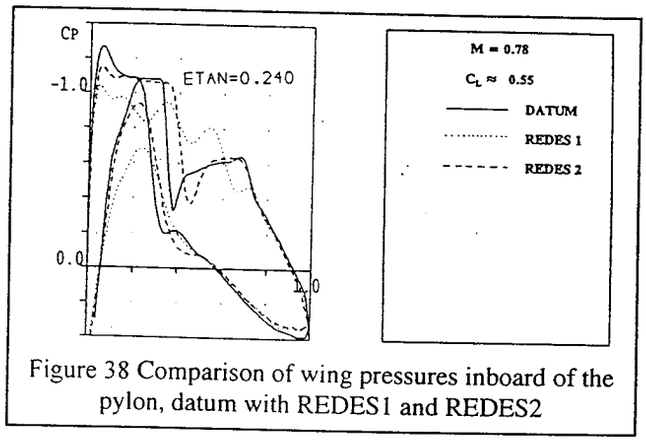

Figure 38 Comparison of wing pressures inboard of the pylon, datum with REDES1 and REDES2

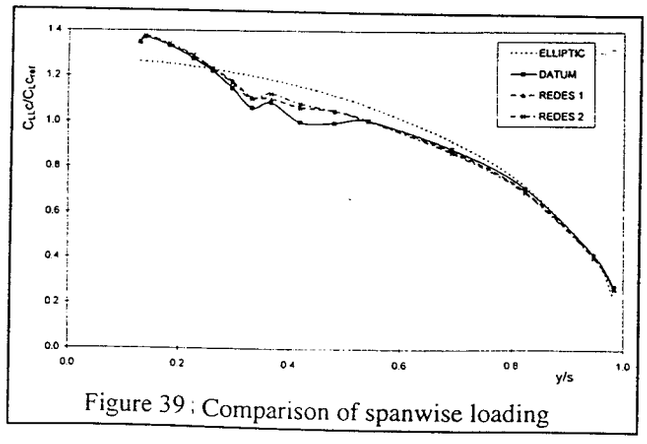

Figure 39 ; Comparison of spanwise loading